



Sohag University



Faculty of Industrial Education

Control Techniques of Induction Motor Drive for Solar Powered Electric Vehicles

A THESIS

Submitted of Electrical Department

Sohag University

in partial fulfillment of the requirement for the degree

MASTER

OF Industrial Education (Power & Machines)

by

Mohammed Abd El-Rahman Abd El-Salam

2018



Sohag University



Faculty of Industrial Education

Control Techniques of Induction Motor Drive for Solar Powered Electric Vehicles

By

Mohammed Abd El-Rahman Abd El-Salam

B.Sc., Electrical Department (Power & Machines), Sohag University

A THESIS

Submitted in partial fulfillment of the requirement for the degree

MASTER

OF Industrial Education (Power & Machines)

SOHAG UNIVERSITY

Sohag, Egypt

2018

Supervision Committee:

Prof. Dr. Farid Naguib Abdelbar

(Faculty of Engineering-Assiut Univ.)

Dr.-Ing. Emad El-Din Hussein Ahmed

(Faculty of Industrial education - Sohag
Univ.)

Discussion Committee:

*To the memory of my beloved father to my
mother, sisters and brothers*

Mohamed Abdelrahman 2018

Acknowledgements

In the name of ALLAH, most Gracious, most Merciful

All deepest thanks are due to **ALLAH**, the merciful, the compassionate for the uncountable gifts given to me.

I would like to express my great thanks to Prof. Dr. **Farid Naguib Abdelbar**, Professor, Electrical Engineering Department, Assiut University for his discussions and encouragement. I would like to express my deepest thanks to him for his kind supervision, generous advice, clarifying suggestions and support during each step of this work. Without his help this thesis would not have been what it is now.

I also would like to express my great thanks to Dr. Ing. **Emad El-Din Hussein Ahmed**, Electrical Department of Industrial Education, Sohag University for his discussions and encouragement.

I would like to thank all the staff members and friends in the Electrical Department, of Industrial Education, Sohag University, for their valuable cooperation that was highly needed during the conduction of this study.

I must not forget to express my deepest thanks to the great, nice, wonderful and lovely family, especially my lovely mother, father, brothers and sisters for their cooperation and support at all stages of this work and against all odds, have been simply overwhelming.

Mohamed Abdelrahman, 2018

Abstract

During the latter part of the 20th century there have been changes which may make the electric vehicle a more attractive proposition. Firstly, there are increasing concerns about the environment, both in terms of overall emissions of carbon dioxide and also the local emission of exhaust fumes which help make crowded towns and cities unpleasant to live in. Secondly there have been technical developments in vehicle design and improvements to rechargeable batteries, motors and controllers.

Generation of electricity from photovoltaic has obtained worldwide acceptance due to its eco-friendly nature and abundant availability. However, we also need solar PV to consider the other electrical systems of the vehicle, the lights, indicators, accessories such as the radio, etc. This availability is subjected to variation owing to many factors such as in shadow, irradiation, temperature etc. Therefore, practical measurements of atmospheric temperature and solar irradiation change are made over several days. The presents evaluation for different control techniques among the most usual maximum power point tracking (MPPT) algorithms. The performance between fuzzy logic and PI controllers with P&O algorithm. This comparison will be made with respect to the amount of energy extracted from photovoltaic (PV), using MATLAB/SIMULINK, dynamic response, and use of sensors. In the experimental setup, a digitally controlled boost DC-DC converter based on P&O algorithm for fuzzy logic and PI controllers, is used to generate PWM pulses for the switches. The main experimental results show the effect of solar irradiation and temperature for conventional MPPT algorithms and improved MPPT algorithm using P&O with fuzzy logic controller. The fuzzy logic controller has merits of its accuracy, reliability, faster dynamic response, and ability to track the global peak power accurately under change in environmental conditions with almost zero steady state oscillations.

Inverter is substantially an interface between DC source like photovoltaic cell and AC networks. There are many doable inverter topologies and switching schemes, and each one will have its own relative benefits and downsides. Efficiency and output current distortion are two necessary factors governing the selection of inverter system, two inverter switching strategies are explored. These are the unipolar and bipolar current controlled inverter employing both the SPWM (Sinusoidal Pulse Width Modulation) and the THPWM (Third Harmonic Pulse Width Modulation) techniques. The models of these techniques are simulated using MATLAB-Simulink software. Simulation results are compared with results of an experimental prototype to confirm validity of results. The results are taken for both static and dynamic loads with different modulation index. Both simulated

and experimental results are in a good agreement. The results showed that the unipolar switched inverter offers low current distortion over bipolar switched inverter.

The constant V/F control method is one of the most common speed control methods for Induction motors (IMs) used in industries. The present thesis studies the V/F control method of induction motor and improves the motor performance with three proposed techniques. The performance of induction motor drive with closed-loop V/F control method using different Pulse Width Modulation (PWM) techniques such as sine triangle Pulse Width Modulation (SPWM), Third-Harmonic Pulse Width Modulation (THPWM) and Space Vector Pulse Width Modulation (SVPWM) is investigated using MATLAB/Simulink. Induction motor is modelled in the synchronous q-d reference frame. The performance of induction motor drive with full load torque is compared using these techniques for total harmonic distortion (THD), harmonics spectra, utilization of DC supply voltage, fundamental peak of the output voltage and motor speed. The dynamic performance of induction motor drive using SVPWM under reference speed and load torque variations are investigated also.

the presents an adaptive (FLC) design technique for controlling an IM speed drive using fuzzy PI control and using only PI controller. which are supplied to SVPWM to generate switching pulses for the inverter switching of IGBTs because low THD the output of voltage, the approach a fitness to attain an optimum trajectory planning, the used of fuzzy logic with PI technique to control the speed of three-phase IM. The use of MATLAB/Simulink to study performance is evaluated in comparison with PI control scheme and FL-PI control the speed of asynchronous machine, the mean absolute error (MAE) of the asynchronous motor speed response is used as a fitness function. The actual velocity of an asynchronous motor is compared with a reference velocity. The mistake is given through FL-PI and PI control, and their outputs control the focal ratio of V/f control is applied to control the voltage magnitude of asynchronous motor. The advantages of V/f control include low-cost because to need speed of IM implementation and the best choices for variable speed and torque applications an optimal FLC based PI control efficiency function is also employed to tune and minimize the mean absolute error to improve the performance of the asynchronous motor in terms of changes in speed and torque. Results obtained from the fuzzy-PI control are compared with those obtained through PI controller to confirm the expanded controller. Results show that the FL-PI controller is better than the PI controllers in all tested cases in terms of damping capability, and transient response under different mechanical loads and speeds and the FL-PI controller is better than the PI controllers TIM applies constant speed and mechanical load variations.

dynamic model of the induction motor in vector control form and characteristic features of the FOC scheme were presented. Mathematical transformations are carried out using Clarke and Park transformations to decouple variables and to facilitate the solutions of complicated equations with time varying coefficients. The simulation of the IFOC scheme is described and the simulation results are presented.

A dynamic simulation model of electric vehicle (EV) was developed using MATLAB/Simulink. The EV model has a configurable structure that is suitable to simulation with multiple fidelity levels. The model has a configurable structure that is suitable to simulation with multiple levels. The powertrain system model developed using MATLAB/Simulink could also be used as a generic, modular and flexible vehicle modeling platform to support the integration of powertrain design and control system optimization.

contents

List of Figures	11
List of Tables	14
List of Symbols	15
List of Abbreviations	18
Introduction	20
1.1 Introduction	20
1.2 Thesis Objectives	22
1.3 Thesis Contents	22
Literature Review	26
2.1 Mechanical Analysis of an Electric Vehicle	26
2.1.1 Tractive Effort	26
2.1.2 Rolling Resistance Force	27
2.1.3 Aerodynamic Drag	28
2.1.4 Hill Climbing Force	28
2.1.5 Acceleration Force	29
2.1.6 Total Tractive Effort	30
2.2 Modeling of Induction Motor	30
2.2.1 Three Phase Induction Machines	31
2.2.2 Machine Model in Arbitrary Reference Frames	33
<i>2.2.2.1 The qdo stationary reference frame equations applicable for motor start up conditions ..</i>	34
<i>2.2.2.2 The qdo synchronous reference frame equations applicable for near synchronous equilibrium motor operation.....</i>	35
2.3 Analysis of Various Methods for Speed Control of Induction Motor	36
2.3.1 Variable Rotor Resistance	37
2.3.2 Variable Stator Voltage	37
2.3.3 Constant V/F Control	38
2.2 Electric Vehicle impacts and performance	39
2.4.1 Economic Impacts	40
2.4.2 Environmental Impacts	40
2.4.3 Grid Impacts	40
2.5 Vehicles and Energy Source	41
2.5.1 Solar Energy	41
2.5.2 Battery for Electric Vehicle	41
<i>2.5.2.1 Lead–Acid Batteries</i>	42
<i>2.5.2.2 Lithium-Ion Batteries</i>	42

2.5.2.3	<i>Nickel–Cadmium (Ni–Cd) Batteries</i>	43
2.6	conclusion	43
Performance Comparison of Fuzzy Logic and PI Controllers Based on MPPT Algorithms for PV systems		44
3.1	Introduction	44
3.2	Modeling of Photovoltaic Cell	45
3.3	Effects of PV Solar on MPP	47
3.3.1	Effects of Solar Irradiance on MPP	48
3.3.2	Effects of temperature on MPP	50
3.4	Maximum Power Point Tracking	51
3.4.1	Power Conversion System.....	51
3.5	Methods of MPPT Algorithms	52
3.5.1	Perturb and Observe Method	52
3.6	Control Technique.....	53
3.6.1	P&O Based on PI	54
3.6.2	P&O Based on Fuzzy Logic.....	54
3.7	Comparison Between Pi and Fuzzy Logic Based on P&O	56
3.8	Conclusion	58
Comparison and Performance Analysis of Unipolar and Bipolar Digitally-Controlled Single-Phase Inverters		59
4.1	Introduction	59
4.2	Circuit Description and Operation	60
4.3	Full- Bridge Single Phase Inverter.....	61
4.3.1	Unipolar Switching Employing SPWM.....	61
4.3.2	Unipolar Switching Employing THPWM	61
4.3.3	Bipolar Switching Employing SPWM.....	62
4.3.4	Bipolar Switching Employing SPWM.....	62
4.4	Static Resistive Load With LC Filter	63
4.4.1	SPWM with Unipolar voltage fed Static Resistive Load	63
4.4.2	THPWM with Unipolar voltage fed Static Resistive Load	64
4.4.3	SPWM with Bipolar voltage fed Static Resistive Load.....	65
4.4.4	THPWM with Bipolar voltage fed Static Resistive Load.....	66
4.5	Dynamic load with LC filter.....	67
4.5.1	Unipolar switching Dynamic load with SPWM	68
4.5.2	Unipolar switching Dynamic load with THPWM	69
4.5.3	Bipolar switching Dynamic load with SPWM	70
4.5.4	Bipolar switching Dynamic load with THPWM	70

4.6	Comparison Between the Four Techniques.....	71
4.6.1	Inverter Fed Static Resistive Load With LC Filter	71
4.6.2	Inverter Fed Dynamic Load With LC Filter	72
4.7	conclusion	72
Comparative Evaluation of PWM Techniques with PI based on V/F Control for Inverter-Fed Induction Motor in electric vehicle Error! Bookmark not defined.		
5.1	Introduction.....	Error! Bookmark not defined.
5.2	Voltage Control of Three-Phase Inverter.....	Error! Bookmark not defined.
5.3.1	Sinusoidal Pulse Width Modulation Technique Description	Error! Bookmark not defined.
5.3.2	Digital Simulation Results for V/F Control Method of Three Phase Induction Motor Using SPWM Technique.....	Error! Bookmark not defined.
5.3.3	Design of PI Controller for the V/F Control Method of Three Phase IM	Error! Bookmark not defined.
5.3.4	Motor Dynamic Performance under Reference Speed Variation	Error! Bookmark not defined.
5.2.4.1	<i>Effect of a Step Change in Reference Speed</i>	Error! Bookmark not defined.
5.2.4.2	<i>Effect of reversal in speed reference</i>	Error! Bookmark not defined.
5.2.5	Motor Dynamic Performance Under Load Torque Variation	Error! Bookmark not defined.
5.2.5.1	<i>Sequential changes in load torque at reference speed of 1200 rpm</i>	Error! Bookmark not defined.
5.2.6	Experimental Results of Induction Motor Using SPWM Technique..	Error! Bookmark not defined.
5.3	Third Harmonic Modulation Technique Description.....	Error! Bookmark not defined.
5.3.1	Digital Simulation Results for V/F control Method of Three Phase Induction Motor Using THPWM Technique.	Error! Bookmark not defined.
5.3.2	Motor Dynamic Performance under Reference Speed Variation	Error! Bookmark not defined.
5.3.2.1	<i>Effect of A Step Change in Reference Speed</i>	Error! Bookmark not defined.
5.3.2.2	<i>Effect of reversal in speed reference</i>	Error! Bookmark not defined.
5.3.3	Motor Dynamic Performance Under Load Torque Variation	Error! Bookmark not defined.
5.3.3.1	<i>Sequential changes in load torque at reference speed of 1200 rpm</i>	Error! Bookmark not defined.
5.3.4	Experimental Results of Induction Motor Using THWM Technique.	Error! Bookmark not defined.
5.4	Space Vector Modulation Technique Description.....	Error! Bookmark not defined.
5.4.1	Determine V_d , V_q , \vec{V}_{ref} , and determine angle (α):.....	Error! Bookmark not defined.
5.4.2	Determine switching time duration $T1$, $T2$, $T0$	Error! Bookmark not defined.

5.4.3	determine Switching time of each transistor [IGPT] (S_1 to S_6).....	Error! Bookmark not defined.
5.4.4	Digital Simulation Results for V/F control Method of Three Phase Induction Motor Using SVPWM Technique.....	Error! Bookmark not defined.
5.4.5	Motor Dynamic Performance under Reference Speed Variation	Error! Bookmark not defined.
5.4.5.1	Effect of A Step Change in Reference Speed	Error! Bookmark not defined.
5.4.5.2	Effect of reversal in speed reference	Error! Bookmark not defined.
5.4.6	Motor Dynamic Performance Under Load Torque Variation	Error! Bookmark not defined.
5.4.6.1	Sequential changes in load torque at reference speed of 1200 rpm	Error! Bookmark not defined.
5.4.7	Experimental Results of Induction Motor Using SVWM Technique .	Error! Bookmark not defined.
5.5	MATLAB Simulink for Comparison Between Three Techniques	Error! Bookmark not defined.
5.5.1	Simulation Results for Starting Characteristic of Full Load Three Phase IM Drive Controlled by the V/F Control Method	Error! Bookmark not defined.
5.5.1.1	Dynamic Performance Comparison of V/F Control Method for Three Types of Modulation Techniques	Error! Bookmark not defined.
5.5.1.2	Effect of Change in Modulation Index on Fundamental Output Voltage and THD	Error! Bookmark not defined.
5.5.1.3	Torque Performance Comparison of V/F Control Method for Three Types of Modulation Techniques	Error! Bookmark not defined.
5.6	Conclusion	Error! Bookmark not defined.
Performance V/F Control by Using Adaptive Fuzzy-PI Controllers for Inverter-Fed Induction Motor		Error! Bookmark not defined.
6.1	Introduction.....	Error! Bookmark not defined.
6.2	General Structure of FLC System	Error! Bookmark not defined.
6.3	Block Diagram of the Proposed Induction Motor Drive Model ...	Error! Bookmark not defined.
6.4	Fuzzy Logic Controller Design.....	Error! Bookmark not defined.
6.5	Membership Function Design	Error! Bookmark not defined.
6.6	Input Linguistic Variables	Error! Bookmark not defined.
6.6.1	Fuzzy sets and Membership Functions for speed error ($e_w(k)$) ...	Error! Bookmark not defined.
6.6.2	Fuzzy sets and Membership Functions for change in speed error ($e_{w(K)}$)	Error! Bookmark not defined.
6.7	Output Linguistic Variables.....	Error! Bookmark not defined.
6.7.1	Fuzzy sets and Membership Functions for FLC output (CF)	Error! Bookmark not defined.

6.8	Rule Base Design for FLC Output	Error! Bookmark not defined.
6.9	Design of the FLC Using MATLAB	Error! Bookmark not defined.
6.9.1	Digital Simulation Results for Adaptive Fuzzy PI Controller	Error! Bookmark not defined.
	6.9.1.1 <i>Effect of A Step Change in Reference Speed</i>	Error! Bookmark not defined.
6.10	Comparison Between the Fuzzy-PI and PI Control Techniques ..	Error! Bookmark not defined.
6.11	conclusion	Error! Bookmark not defined.
A Comparative Analysis of Scalar V/F and Vector Control with PI of Induction Motor Drive		
7.1	introduction	Error! Bookmark not defined.
7.2	Description of Vector Control or Field Oriented Control	Error! Bookmark not defined.
7.3	Determination of the Rotor Flux Angle.....	Error! Bookmark not defined.
7.4	Basic Scheme of Field Oriented Control of Induction Motor	Error! Bookmark not defined.
	7.4.1 Direct Field Oriented Control	Error! Bookmark not defined.
	7.4.2 Indirect Field Oriented Control	Error! Bookmark not defined.
7.5	Clarke Transformation.....	Error! Bookmark not defined.
7.6	Park Transformation.....	Error! Bookmark not defined.
7.7	Inverse Park Transformation.....	Error! Bookmark not defined.
7.8	Block Diagram of the Proposed IFOC of Induction Motor Drive Model	Error! Bookmark not defined.
7.9	Simulation Results for IFOC of Induction Motor Drive	Error! Bookmark not defined.
7.9.1	Motor Dynamic Performance under Reference Speed Variation	Error! Bookmark not defined.
	7.9.1.1 <i>Effect of A Step Change in Reference Speed</i>	Error! Bookmark not defined.
	7.9.1.2 <i>Effect of reversal in speed reference</i>	Error! Bookmark not defined.
	7.9.1.3 <i>Effect of A Step Change in Reference Ramp Speed</i>	Error! Bookmark not defined.
7.9.2	Motor Dynamic Performance Under Load Torque Variation	Error! Bookmark not defined.
	7.9.2.1 <i>Sequential changes in load torque at reference speed of 400 rpm</i>	Error! Bookmark not defined.
7.10	comparison of THD with PI, FL-PI control, IFOC models' performance in multistep speed response	Error! Bookmark not defined.
7.11	Conclusion	Error! Bookmark not defined.
Design and Dynamics Modeling for Electric Vehicle		
8.1	Introduction.....	Error! Bookmark not defined.
8.2	Gear block	Error! Bookmark not defined.

8.3	Tire block	Error! Bookmark not defined.
8.4	Vehicle body block	Error! Bookmark not defined.
8.5	Driving Cycles.....	Error! Bookmark not defined.
8.6	Range modelling of battery electric vehicles.....	Error! Bookmark not defined.
8.6.1	Principles of battery electric vehicle modelling	Error! Bookmark not defined.
8.6.2	Modelling equations	Error! Bookmark not defined.
8.7	Simulation of MATLAB and Prototype	Error! Bookmark not defined.
8.7.1	Simulation Results and Interpretation.....	Error! Bookmark not defined.
8.8	Conclusion	Error! Bookmark not defined.
	Conclusions and Suggestions for Future Work	Error! Bookmark not defined.
9.1	Introduction.....	Error! Bookmark not defined.
9.2	Conclusion	Error! Bookmark not defined.
9.3	Future Work	Error! Bookmark not defined.
	appendix.....	Error! Bookmark not defined.
	Appendix (A1)Err
	or! Bookmark not defined.	
	Appendix (A2)Err
	or! Bookmark not defined.	
	Appendix (A3)Err
	or! Bookmark not defined.	
	Appendix (A4)Err
	or! Bookmark not defined.	
	Appendix (B1)Err
	or! Bookmark not defined.	
	Appendix (B2).....	Error! Bookmark not defined.
	Appendix (B3)Err
	or! Bookmark not defined.	
	Appendix (C1)Err
	or! Bookmark not defined.	
	Appendix (C2)Err
	or! Bookmark not defined.	
	References	Error! Bookmark not defined.
	List of publications.....	Error! Bookmark not defined.

List of Figures

Fig 2.1: The forces acting on a vehicle moving along a slope 27
Fig 2.2: The pressure distribution of the contact area between tire and road at standstill on a leveled hard road surface..... 28
Fig 2.3: A simple arrangement for connecting a motor to a drive wheel 29

Fig 2.4: Idealized circuit model of three phase induction machine, showing the rotating stator magnetic field and the mechanically rotating rotor.	31
Fig 2.5: Relationship between ABC and qdo arbitrary coordinate reference frames.....	33
Fig 2.6: Torque-speed characteristics of a 3 – ϕ IM with variable rotor resistance.	37
Fig 2.7: Torque-speed characteristics of a 3 – ϕ IM with variable stator voltage.....	38
Fig 2.8: Torque-speed characteristics of a 3 – ϕ IM with constant V/F method.	38
Fig 2.9: Wh/Kg for various battery types.....	42
Fig 3.1: Equivalent Simplified circuit of a photovoltaic cell.	45
Fig. 3.2 a: as shown the measurement devices such as solar radiation, temperature measurement, variable resistance, and PV module.....	47
Fig. 3.3: Experimental results of variation of irradiation and temperatures from 6 am to 6 pm in Sohag city	48
Fig. 3.2 b: Experimental prototype using PV solar of electric vehicle.....	48
Fig. 3.4: I-V and P-V curves of the PV module under various values of irradiation (100, 500, 1000 W/m ²).	49
Fig. 3.5: Experimental results of variation of irradiation and temperatures from 6 am to 6 pm P-V power characteristic for different irradiation and temperature levels in Sohag city fig (c).....	49
Fig. 3.6: IV and PV curves of the PV module under various values of temperature (0, 25, 50, 100 C°)	50
Fig. 3.7: P-V curve for fast irradiation change from A [low point] to D or C [high point] to problem P&O- MPPT.....	53
Fig. 3.7: MPPT using fuzzy logic and PI control based on P&O method MATLAB Simulink.	54
Fig. 3.8: surface of FLC absolute output 3D as a function of the two inputs.....	55
Fig. 3.9: irradiation and comparison between output voltage used fuzzy logic and PI under varying fast change irradiation.	56
Fig 3.10: comparison between output power used fuzzy logic and PI under varying fast change irradiation	57
Fig 3.11: temperature and comparison between output voltage used fuzzy logic and PI under varying fast change temperature.	57
Fig 3.12: comparison between output power used fuzzy logic and PI under varying fast change temperature.....	57
Fig 4.1: Inverter circuit with LC filter	60
Fig. 4.2: Unipolar switching with SPWM.....	61
Fig. 4.3: Unipolar switching with THPWM	62
Fig. 4.4: Bipolar switching with SPWM.....	62
Fig. 4.5: Bipolar switching with THPWM	63
Fig. 4.6: A picture for the experimental prototype.....	63
Fig. 4.7: Experimental switching pulses for unipolar switching	64
Fig. 4.8: Simulated output voltage with SPWM with LC filter	64
Fig. 4.10: FFT for unipolar switching with SPWM.....	64
Fig. 4.9: Experimental output voltage with SPWM with LC filter	64
Fig. 4.12: Simulated output voltage with LC filter	65
Fig. 4.11: Experimental switching pulses for unipolar switching with THPWM.....	65
Fig. 4.13: Experimental output voltage	65
Fig. 4.14: FFT for unipolar switching with THPWM	65
Fig. 4.16: Simulated output voltage	66
Fig. 4.15: Experimental switching pulses for bipolar switching with SPWM.....	66
Fig. 4.18: FFT for bipolar switching with SPWM.....	66
Fig. 4.17: Experimental output voltage	66
Fig. 4.20: Simulated output voltage with LC filter	67
Fig. 4.19: Experimental switching pulses for bipolar switching with THPWM	67
Fig. 4.22: FFT for bipolar switching with THPWM	67
Fig. 4.21: Experimental output voltage with LC filter	67

Fig. 4.23: A picture for the experimental prototype single phase inverter	68
Fig. 4.25: FFT for unipolar switching with SPWM.....	68
Fig. 4.24: Simulated output current with LC filter for unipolar switching with SPWM	68
Fig. 4.26: Experimental output current with LC filter for unipolar switching with SPWM	69
Fig. 4.28: FFT for unipolar switching with THPWM	69
Fig. 4.27: Simulated output current with LC filter for unipolar switching with THPWM.....	69
Fig. 4.29: Experimental output current with LC filter for unipolar switching with THPWM.....	69
Fig. 4.31: FFT for Bipolar switching with SPWM	70
Fig. 4.30: Simulated output current with LC filter for Bipolar switching with SPWM	70
Fig. 4.32: Experimental output current with LC filter for Bipolar switching with SPWM	70
Fig. 4.34: FFT for Bipolar switching with THPWM	71
Fig. 4.33: Simulated output current with LC filter for Bipolar switching with THPWM.....	71
Fig. 4.35: Experimental output current with LC filter for Bipolar switching with THPWM.....	71
Fig. 4.36: THD for static resistive load with LC filter	72
Fig. 4.37: THD for dynamic load with LC filter	72
Fig 5.1: Comparison between sinusoidal and triangular waveform and pulses to switches TA+ and TA- for line voltage V ab	Error! Bookmark not defined.
Fig 5.2: Block diagram of V/F control method of three phase IM using SPWM technique.....	Error! Bookmark not defined.
Fig 5.3: SPWM technique using MATLAB/Simulink	Error! Bookmark not defined.
Fig 5.4: Calculation of modulation index for the inverter	Error! Bookmark not defined.
Fig 5.5: Implementation of single phase rectifier and three phase inverter fed induction motor.	Error! Bookmark not defined.
Fig 5.6: gate drive operation (IGPT) Type of (80N60) fed three phase induction motor	Error! Bookmark not defined.
Fig 5.7: Motor performance for step change in reference speed.....	Error! Bookmark not defined.
Fig 5.8: Motor performance for speed reversal due to change in speed reference	Error! Bookmark not defined.
Fig 5.9: Motor performance for sequential change in load torque.	Error! Bookmark not defined.
Fig 5.10: Experimental line and phase voltage of induction motor using SPWM.	Error! Bookmark not defined.
Fig 5.11: Increasing fundamental output voltage by addition of third harmonic .	Error! Bookmark not defined.
Fig 5.12: Block diagram of V/F control method of three phase IM using THPWM technique. ..	Error! Bookmark not defined.
Fig 5.13: THPWM MATLAB model	Error! Bookmark not defined.
Fig 5.14: Motor performance for step change in reference speed.....	Error! Bookmark not defined.
Fig 5.15: Motor performance for speed reversal due to change in speed reference....	Error! Bookmark not defined.
Fig 5.17: Motor performance for sequential change in load torque.	Error! Bookmark not defined.
Fig 5.18: Experimental line and phase voltage of induction motor using THWM	Error! Bookmark not defined.
Fig 5.19: Three-phase voltage source PWM inverter.....	Error! Bookmark not defined.
Fig 5.20: Locus comparison of maximum linear control voltage in SPWM and SVPWM.....	Error! Bookmark not defined.
Fig 5.21: The relationship of abc reference frame and stationary dq reference frame	Error! Bookmark not defined.
Fig 5.22: Basic switching vectors and sectors	Error! Bookmark not defined.
Fig 5.23: Reference vector as a combination of adjacent vectors at sector 1.	Error! Bookmark not defined.
Fig 5.24: Space vector PWM switching patterns at each sector.....	Error! Bookmark not defined.
Fig 5.24: Space vector PWM modulation.....	Error! Bookmark not defined.

Fig 5.25: Block diagram of V/F control method of three phase IM using SVPWM techniqueError! Bookmark not defined.

Fig 5.26: SVPWM technique using MATLAB/SimulinkError! Bookmark not defined.

Fig 5.27: Motor performance for step change in reference speed.....Error! Bookmark not defined.

Fig 5.28: Motor performance for speed reversal due to change in speed reference....Error! Bookmark not defined.

Fig 5.29: Motor performance for sequential change in load torque.Error! Bookmark not defined.

Fig 5.30: Experimental line and phase voltage of induction motor using SVWM Error! Bookmark not defined.

Fig 5.31: Simulink model for overall system.....Error! Bookmark not defined.

Fig 5.32: by Changing motor speed performance for different PWM techniques Error! Bookmark not defined.

Fig 5.33: comparison THD motor performance for different PWM techniques...Error! Bookmark not defined.

Fig 5.34: by Changing motor torque performance for different PWM techniquesError! Bookmark not defined.

Fig 5.1: General structure of fuzzy inference system.Error! Bookmark not defined.

Fig 6.2: Block diagram of adaptive FL-PI V/F control method for induction motor drive.....Error! Bookmark not defined.

Fig 6.3: Fuzzy sets and the respective membership functions for speed error ($e_w(k)$).Error! Bookmark not defined.

Fig 6.4: Fuzzy sets and the respective membership functions for change in speed error ($ce_w(k)$).Error! Bookmark not defined.

Fig 6.5: Fuzzy sets and the respective membership functions for FLC output (CF)...Error! Bookmark not defined.

Fig 6.6: MATLAB adaptive fuzzy logic PI with constant V/F control model.Error! Bookmark not defined.

Fig 6.7: Motor performance for step change in reference speed.....Error! Bookmark not defined.

Fig 6.8: speed response of IM with FL-PI and PI control V/F speed various in steps Error! Bookmark not defined.

Fig 6.9: torque response of IM with FL-PI and PI control V/F torque various in steps.....Error! Bookmark not defined.

Fig 7.1: Field orientation in d-q reference frameError! Bookmark not defined.

Fig. 7.2: Direct field-oriented control drive system.....Error! Bookmark not defined.

Fig. 7.3: Indirect field-oriented control drive system.....Error! Bookmark not defined.

Fig. 7.4: Stator current space vector in stationary reference frameError! Bookmark not defined.

Fig. 7.5: Stator current space vector in rotating reference frameError! Bookmark not defined.

Fig. 7.6: Stator voltage space vector from d-qError! Bookmark not defined.

Fig 7.7: Block diagram of indirect field-oriented control of induction motor model..Error! Bookmark not defined.

Fig 7.8: PI with IFOC of three phase induction motor using MATLAB/Simulink.....Error! Bookmark not defined.

Fig 7.9: Motor performance for step change in reference speed.....Error! Bookmark not defined.

Fig 7.10: Motor performance for speed reversal due to change in speed reference....Error! Bookmark not defined.

Fig 7.11: Motor performance for step change in reference ramp speed ..Error! Bookmark not defined.

Fig 7.12: Motor performance for sequential change in load torque.Error! Bookmark not defined.

Fig. 8.1: The structural component of differential block.....Error! Bookmark not defined.

Fig. 8.2: Scheme of the vehicle modelError! Bookmark not defined.

Fig. 8.3: Vehicle model.....Error! Bookmark not defined.

Fig 8.4: European driving scheduleError! Bookmark not defined.

Fig 8.5: Energy flows in the ‘classic’ battery powered electric vehicle, which has regenerative brakingError! Bookmark not defined.

fig 8.6: The simulation of MATLAB and prototype of electric vehicleError! Bookmark not defined.
fig 8.7: Mechanical speed of electric vehicle.Error! Bookmark not defined.
Fig 8.8: Speed of induction motor (rpm).Error! Bookmark not defined.
Fig 8.9: Stator phase current of induction motor under varies speedError! Bookmark not defined.
Fig 8.10: Torque with shows angular speed under mechanical speed of electric vehicle.Error!
Bookmark not defined.
Fig 9.1: FIS editor: rules window in MATLAB.Error! Bookmark not defined.
Fig 9.2: Membership functions of speed error (ew(k)).Error! Bookmark not defined.
Fig 9.3: Membership functions of change in error (cew(k)).Error! Bookmark not defined.
Fig 9.4: Membership functions of change in frequency.Error! Bookmark not defined.
Fig 9.5: Three-dimensional plot of the control surface.Error! Bookmark not defined.
Fig 10.6: outputs for different inputs.Error! Bookmark not defined.

List of Tables

Table 3.1: Electrical parameter of the PV module 47
Table 3.2: fuzzy rules that are used FL-MPPT 55
Table 4.1: Specifications with static load 63
Table 4.2: Specifications with dynamic load 68
Table 5.1: Parameter of PI controllerError! Bookmark not defined.
Table 5.2: Switching vectors, phase voltages and output line to line voltages.Error! Bookmark not defined.
Table5.3. switching time calculation at each sector:Error! Bookmark not defined.
Table 6.1: Fuzzy rule base of FLCError! Bookmark not defined.
Table 6.2: Parameters of PI controllerError! Bookmark not defined.
Table 6.3: A comparison of PI, and FL-PI control models' performance in multistep speed response.Error! Bookmark not defined.
Table 6.4: A comparison of THD with PI, and FL-PI control models' performance in multistep speed response.Error! Bookmark not defined.
Table 7.1: Parameters of the used PI controller with IFOC of induction motor...Error! Bookmark not defined.
Table 7.2: A comparison of THD with PI, and FL-PI control models' performance in multistep speed response.Error! Bookmark not defined.
Tab. 8.1: The tire model variablesError! Bookmark not defined.
Table 8.2: The vehicle motion model variables.....Error! Bookmark not defined.
Table 8.3: Vehicle dynamicsError! Bookmark not defined.
Table 8.4: Determine the total power used in prototype electric vehicle .Error! Bookmark not defined.
Table 8.5: Different total Weight of electric vehicle and power of induction motor ...Error! Bookmark not defined.
Table 9.1: The parameters of 3-phase IM1 that we used in simulation. ..Error! Bookmark not defined.

List of Symbols

f	is the rated frequency of the motor
P	is the number of pole
s	is the per unit slip
ω_r	is the rotor speed
ω_e	is the synchronous reference speed
ω_b	is the base speed
ω_{sl}	is the slip frequency
ω_{sr}	is the rated slip speed
V_s	is the stator terminal voltage
R_s	is the stator resistance
R_r'	is the rotor resistance
R_r	is the rotor-reflected resistance
x_m	is the magnetizing reactance
x_{ls}	is the stator leakage reactance
x_{lr}'	is the rotor leakage reactance
L_{lr}'	is the rotor leakage inductance
L_{ls}	is the stator leakage inductance
L_{lr}	is the rotor-reflected leakage inductance

L_m	is the magnetizing inductance
L_{ms}	is the magnetizing inductance for the stator
L_{mr}	is the magnetizing inductance for the rotor
L_{sr}	is the amplitude of the mutual inductance between stator and rotor
L_s	is the single equivalent stator wire coil inductance
L_r	is the single equivalent rotor wire coil inductance
i_o	is the load current
I_m	is the magnetizing component current
I_r	is the rotor-reflected current
I_s	is the stator current
E_{ar}	is the rated induced e.m.f
T_{mr}	is the rated torque
f_{slip}	is the slip frequency
K_e, K_h	is the core coefficients
$P_{(Air-gap3\Phi)}$	is the air-gap power
s_r	is the motor rated slip
v_{as}, v_{bs}, v_{cs}	is the stator three-phase input voltages
i_{as}, i_{bs}, i_{cs}	is the three-phase stator current
v_{ar}, v_{br}, v_{cr}	is the induced rotor three-phase voltages
i_{ar}, i_{br}, i_{cr}	is the three-phase rotor current
V_{ab}, V_{bc}, V_{ca}	is the line-line voltage
V_{an}, V_{bn}, V_{cn}	is the phase voltage
V_o	is the offset voltage
$T_{qdo}(\theta)$	is the associated torque transformation matrix
θ_r	is the rotor angle
λ	is the flux linkage
v_{qs}^s, v_{ds}^s	is the quadrature and direct stator voltage components in stationary reference frame
ψ_{qs}^s, ψ_{ds}^s	is the quadrature and direct stator flux linkage per second component in stationary reference frame
i_{qs}^s, i_{ds}^s	is the quadrature and direct stator current components in stationary reference frame
ψ_{qr}^s, ψ_{sr}^s	is the quadrature and direct rotor linkage per second component in stationary reference frame

i'_{qr}, i'_{dr}	is the quadrature and direct rotor current components in stationary reference frame
ψ_{qs}^e, ψ_{ds}^e	is the quadrature and direct stator flux linkage per sec components in rotating reference frame
i_{qs}^e, i_{ds}^e	is the quadrature and direct stator current components in rotating reference frame
ψ'_{qr}, ψ'_{dr}	is the quadrature and direct rotor flux linkage per second components in rotating reference frame
i'_{qr}, i'_{dr}	is the quadrature and direct rotor current components in rotating reference frame
\hat{V}_{tr}	is the amplitude of triangular waveform
f_s	is the carrier frequency or switching frequency
$v_{control}$	is the control signal
f_1	is the desired fundamental frequency or modulating frequency
m_a	is the amplitude modulation ratio
m_f	is the frequency modulation ratio
$\hat{V}_{control}$	is the amplitude of control signal
V_{DC}	is the DC link voltage of the inverter
V_{Ao}	is the output voltage of the inverter
V_{ref}	is the desired reference voltage vector
T_0, T_1, T_2	is the switching time duration for states at any sector
T_s	is the switching time
$V_0:V_7$	is the eight inverter voltage vectors
K	is a factor for increasing the amplitude of the reference wave form in THPWM technique
$ew(K)$	is the motor speed error
$cew(K)$	is the change in speed error
$w_r^*(k)$	is the reference speed
$w_r(k)$	is the actual rotor speed
$ew(k-1)$	is the value of error at previous sampling time

List of Abbreviations

AC	Alternating Current
EV	Electric vehicle
AFPIC	Adaptive Fuzzy PI controller
BJTs	Bipolar Junction Transistors
CFI	Current-Fed Inverters
DC	Direct Current
DSP	Digital Signal Processing
EMF	Electromagnetic Force
FLC	Fuzzy Logic Controller
FPGA	Field Programmable Gate Array
FFT	Fast Fourier Transform
GTOs	Gate-Turn-off Thyristors
HP	Horse Power
IM	Induction Motor

IGBTs	Insulated-Gate Bipolar Transistors
MOSFETs	Metal Oxide Semiconductor Field-Effect Transistors
MCTs	Metal Oxide Semiconductor-Controlled Thyristor
PWM	Pulse Width Modulation
rpm	Revolution per minute
SCIM	Squirrel Cage Induction Motor
SRIM	Slip Ring Induction Motor
SITs	Static Induction Transistors

Introduction

1.1 Introduction

The modern society is highly dependent on personal transportation. A large market within this area is the passenger car. In 2008 approximately 53 million cars were produced worldwide. The main type of passenger cars is the internal combustion engine vehicle (ICEV). The increasing number of ICEVs worldwide entails an increase in pollution of the environment and contributes to the depletion of the oil resources[1].

The commercial electric vehicles were available by the end of the 19th century. The electric vehicle (EV) has now entered its third century as a commercially available product and as such it has been very successful, outlasting many other technical ideas that have come and gone. However, electric vehicles have not enjoyed the enormous success of internal combustion (IC) engine vehicles that normally have much longer ranges and are very easy to refuel. Today's concerns about the environment, particularly noise and exhaust emissions, coupled to new developments in batteries and fuel cells may swing the balance back in favor of electric vehicles. It is therefore important that the principles behind the design of electric vehicles, the relevant technological and environmental issues are thoroughly understood[2].

Power electronics deals with conversion and control of electrical power in the wide range of milliwatts to gigawatts with the help of switching mode power semiconductor devices[3]. The applications of power electronics may include Direct Current (DC) and AC regulated power supplies, uninterruptible power supply (UPS) systems, electrochemical processes, heating and lighting control, electronic welding, power line static VAR compensators [SVCs, static VAR generator, or static synchronous compensator (STATCOM)], active harmonic filters, high voltage DC (HVDC) systems, photovoltaic (PV) and fuel cell (FC) power conversion, solid state DC and AC circuit breakers, high-frequency heating, and motor drives. Motor drives area may include applications in computers and peripherals, solid state starters for motors, transportation (electric/hybrid electric vehicles (EV/HEV), subway, etc.), home appliances, paper and textile

mills, wind generation system, air-conditioning and heat pumps, rolling and cement mills, machine tools and robotics, pumps and compressors, ship propulsion, etc. In addition to applications in energy systems and industrial automation, power electronics is now playing a significant role in global energy conservation that is indirectly helping in the environmental pollution control, i.e., solving the global warming problem[4].

Over the past decades DC machines were used extensively for variable speed applications due to the decoupled control of torque and flux that can be achieved by armature and field current control respectively. DC drives are advantageous in many aspects as in delivering high starting torque, ease of control and nonlinear performance. But due to the major drawbacks of DC machine such as presence of mechanical commutator and brush assembly, DC machine drives have become obsolete today in industrial applications, the robustness, less expensive, the better performance and the ease of maintenance make the asynchronous motor advantageous in many industrial applications or general applications. IMs are the most widely used motors in domestic appliances, industrial control, and automation. Hence, they are often called the workhorse of the motion industry. It is available from several watts single phase small motor designs, IMs evolved to tens thousands of horse power (746 Watts/HP) driven by three phase mains voltages [5].

There are two types of rotor windings, are wounded rotor and squirrel-cage rotor. The Squirrel Cage Induction Motors (SCIM) are more widely used than all the rest of the electric motors as they have all the advantages of Alternating Current (AC) motors and are cheaper in cost as compared to Slip Ring Induction motors (SRIM); require less maintenance and rugged construction. Because of the absence of slip rings, brushes maintenance duration and cost associated with the wear and tear of brushes are minimized. Due to these advantages, the IMs have been the execution element of most of the electrical drive system for all related aspects: starting, braking, speed change and speed reversal etc. [5].

Industrial drive applications are generally classified into constant speed and variable speed drives. Traditionally AC machines have been used in constant speed applications, whereas DC machines were preferred for variable speed drives. DC machines have the disadvantages of higher cost and maintenance problems with commutators and brushes. Commutators and brushes do not permit a machine to operate in dirty and explosive environment. An AC machine overcomes the drawback of DC machines. Although currently, the majority of variable speed drive applications use DC machines, they are progressively being replaced by AC drives. When power is supplied to an IMs, it runs at its rated speed. However, many applications need variable speed operations. For example, an electric vehicle (EV) may use different speeds for each speed cycle. Historically, mechanical gear systems were used to obtained variable speed. Recently, power electronics and control

systems have matured to allow these components to be used for motor control in place of mechanical gears[6].

The growing energy demand is coupled with the possibility of lower supply of conventional fuels[7]. Moreover, with growing concerns about environmental conservation, the electrical energy from solar (PV) cells fed lighting in electric vehicle is currently regarded as a natural energy source that is more useful. This is due to that it is free, abundant, clean, distributed over the Earth, and contribute as a primary factor of all other processes of energy production. The used MPPT techniques are important to extract the maximum power available in solar PV[8]. Therefore, the operating current and voltage which maximize power output will be varied with environmental conditions, the perturbation and observation P&O, the IC methods based on fixed iteration step size are simple and have good performances. Therefore, they are characterized by slow convergence, oscillations in the PV power around the MPP, operation failure under rapidly changing atmospheric temperature, and irradiation conditions. Using small perturbation step size will result in reduced oscillations, but the speed of tracking MPPT remains slower. To acquire a fast response speed and to overcome the aforementioned drawbacks, a modified MPPT algorithms with variable step size have been the subject of many investigations. Generally, the conventional (IC) MPPT algorithm uses a fixed step size and oscillation can be reduced to track the (MPP)[9], [10].

1.2 Thesis Objectives

The thesis objectives are summarized as follows:

1. Mechanical analysis of an electric vehicle using MATLAB/Simulink.
2. Performance comparison of fuzzy logic and pi controllers based on MPPT algorithms for PV systems.
3. Comparison and Performance Analysis of Unipolar and Bipolar Digitally-Controlled Single-Phase Inverters.
4. Modeling V/F control method of three phase IM with different PWM techniques as SPWM, THPWM and SVPWM with the help of MATLAB/Simulink.
5. Introducing a FL-PIC to improve the performance of V/F control for three phases IM using MATLAB/Simulink.
6. A comparative analysis of scalar v/f and vector control with pi of induction motor drive.
7. Design and dynamics modeling for electric vehicle.

1.3 Thesis Contents

To achieve the above objectives, the presented thesis is organized in nine chapters in additions to the list of references and appendixes, the chapters are organized as follows:

Chapter 1 is titled "Introduction". It demonstrates electric vehicle and power electronics technology and its application. presents a comparison between DC an AC machine, solar (PV) cells fed lighting of electric vehicle is currently important to extract the maximum power available in solar PV and introduces summary about each chapter and its contents.

Chapter 2 is titled "literature Review". It introduces mechanical analysis of an EV is presented to determine the forces acting on it when driving and modeling of three phase induction motor, based on battery is sized in its capacity to provide enough energy to last a typical drive period in a day.

Chapter 3 is titled " Performance Comparison of Fuzzy Logic and PI Controllers Based on MPPT Algorithms for PV systems". A novel maximum power point tracking technique based on FL-MPPT PV system has been presented, which has the ability to track the MPP when there are big fluctuations of irradiation. The advantages and disadvantages of the FL-MPPT and P&O-MPPT have been discussed. The designed membership functions of FL the controller where tuned based on modified a P&O algorithm to incorporate the advantages of the PI-MPPT and the FL-MPPT as well as to eliminate their drawbacks. A MATLAB-SIMULINK model for the PV system was developed. The P&O-MPPT, FL-MPPT, PI-MPPT and proposed method were simulated, being then compared, according to their common features.

Chapter 4 is titled " Comparison and Performance Analysis of Unipolar and Bipolar Digitally-Controlled Single-Phase Inverters". A comparison between unipolar and bipolar PWM techniques is introduced employing SPWM and THPWM with various modulation ratio. The comparison between the presented four topologies is presented for static and dynamic loads. The models of these topologies are implemented by simulations and an experimental prototype. For static load, SPWM technique with unipolar switching gives the least THD whereas SPWM technique with bipolar switching gives THD less than THPWM technique with unipolar switching. For dynamic load, also SPWM technique with unipolar switching gives the least THD whereas THPWM technique with unipolar switching gives THD less than SPWM technique with bipolar switching.

Chapter 5 is titled " Comparative Evaluation of PWM Techniques with PI based on V/F Control for Inverter-Fed Induction Motor in electric vehicle". A comparison PWM techniques with PI for three-phase inverter-fed IM. Space-vector Modulation Technique is most popular and of much importance among all the PWM techniques for three-phase inverter-fed induction motor. The simulation and experimental results reveal that SVPWM gives 15% increase in the fundamental output with better quality i.e. lesser THD compared to SPWM or THPWM. This can be observed

in the comparison made between the three techniques for different modulation ratio. PWM techniques comprising SPWM, THPWM, and SVPWM are implemented in MATLAB/SIMULINK software and also an experimental prototype is implemented.

Chapter 6 is titled " presents an adaptive (FLC) design technique for controlling an IM speed drive using fuzzy PI control and using only PI controller. which are supplied to SVPWM to generate switching pulses for the inverter switching of IGBTs because low THD the output of voltage, the approach a fitness to attain an optimum trajectory planning, the used of fuzzy logic with PI technique to control the speed of three-phase IM. The use of MATLAB/Simulink to study performance is evaluated in comparison with PI control scheme and FL-PI control the speed of asynchronous machine, the mean absolute error (MAE) of the asynchronous motor speed response is used as a fitness function. The actual velocity of an asynchronous motor is compared with a reference velocity. The mistake is given through FL-PI and PI control, and their outputs control the focal ratio of V/f control is applied to control the voltage magnitude of asynchronous motor. The advantages of V/f control include low-cost because to need speed of IM implementation and the best choices for variable speed and torque applications an optimal FLC based PI control efficiency function is also employed to tune and minimize the mean absolute error to improve the performance of the asynchronous motor in terms of changes in speed and torque. Results obtained from the fuzzy-PI control are compared with those obtained through PI controller to confirm the expanded controller. Results show that the FL-PI controller is better than the PI controllers in all tested cases in terms of damping capability, and transient response under different mechanical loads and speeds and the FL-PI controller is better than the PI controllers TIM applies constant speed and mechanical load variations.

Chapter 7 is titled " A Comparative Analysis of Scalar V/F and Vector Control with PI of Induction Motor Drive". Fast response of vector control makes it better than other method of speed control of induction motor. By using this method, we attend maximum response in minimum time. By result analysis change in load torque speed attend reference speed in minimum time, by comprise with scalar control method this method is fast accurate and control variable speed of induction motor. We can control speed by varying parameters of motor, load torque, load limit value. Its sharp and accurate function of flux and speed control. By redefining the maximum torque and acceleration limit parameters the rise time could also be modified easily. The degraded performance for a sampling time Scalar control is simple to implement, but the inherent coupling effect (that is both the flux and the torque are functions of voltage or current and frequency) gives sluggish response and the system is prone to instability because of a high order system effect. If

the torque is increased by incrementing the slip or frequency the flux tends to decrease and this flux variation is very slow. The flux decrease is then compensated by the flux control loop, which has a large time constant.

Chapter 8 is titled " Design and Dynamics Modeling for Electric Vehicle". The methodology for designing the propulsion and driving system using the Simulink program has been presented. The analyzed driving system was divided into functional components: engine, gearbox and powertrain with rubber wheels. For each component, key features and model limitations were identified. The basic formulas and the mathematical relationships used in modeling have been demonstrated. Mathematical formulas are written in a parametric manner using coefficients. The coefficients values are given for the calculation of the propulsion engine, the driving wheels and the dynamic effects on the vehicle. The equations described above allow for quick analysis of the output when changing certain coefficients.

Chapter 9 is titled " Conclusions and Suggestions for Future Work". It reports the main conclusion that can be drawn from the thesis as a whole and summarizes the proposed future research work in the area of control techniques of induction motor drive for solar powered electric vehicles.

Literature Review

2.1 Mechanical Analysis of an Electric Vehicle

With all vehicles the prediction of performance and range is important. Computers allow us to do this reasonably easily. Above all, computer-based methods allow us to quickly experiment with aspects of the vehicle, such as motor power, battery type and size, weight and so on, and see how the changes affect the performance and range. The first parameter we will model is vehicle performance. By performance we mean acceleration and top speed, an area where electric vehicles have a reputation of being very poor. It is necessary that any electric vehicle has a performance that allows it, at the very least, to blend safely with ordinary city traffic. Many would argue that the performance should be at least as good as current IC engine vehicles if large scale sales are to be achieved. The first step in vehicle performance modelling is to produce an equation for the tractive effort. This is the force propelling the vehicle forward, transmitted to the ground through the drive wheels[11].

2.1.1 Tractive Effort

In this section a mechanical analysis of an EV is presented to determine the forces acting on it when driving. The analysis also applies for an ICEV. In figure 2.1. The initial testing is conducted in accordance with the scenario. Analysis of electric vehicle is required to get the suitable size of the induction motor and battery source. First step is the modeling to make an equation of tractive effort to determine how much load on the electric vehicle to a flat road condition. The tractive effort on electric vehicle include rolling resistance force, aerodynamic drag, hill climbing force and acceleration force should be studied further. The rolling resistance force is thrust into the front of the electric vehicle[12]. This is equal to the transmitting wheel to be through a street like Fig 2.1 a diagram displaying the forces acting on a rear-wheel driven EV driving uphill is seen. The forces acting against the direction of motion of the EV are the gravity ($mg \cdot \sin(\theta \text{ road})$), the aerodynamic drag F_{ad} and the rolling resistance force F_{rr} . The force acting in direction of the motion is the traction force F_a .

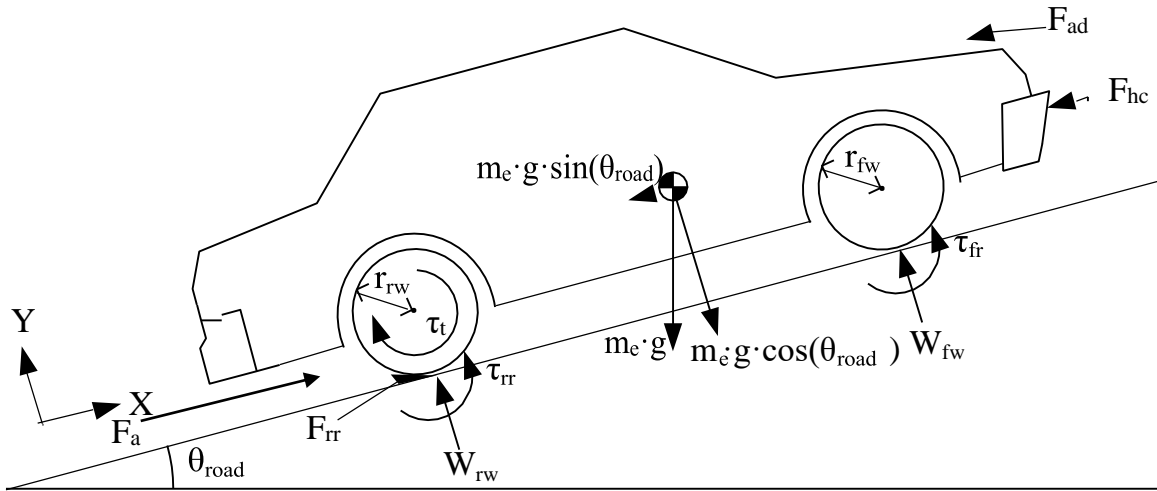


Fig 2.1: The forces acting on a vehicle moving along a slope

2.1.2 Rolling Resistance Force

The rolling resistance is primarily due to the friction of the vehicle tire on the road. Friction in bearings and the gearing system also play their part[13]. The rolling resistance is approximately constant, and hardly depends on vehicle speed. It is proportional to vehicle weight. The equation is:

$$F_{rr} = \mu_{rr} mg \quad (2.1)$$

where:

F_{rr}	Rolling Resistance [N]
μ_{rr}	Rolling resistance coefficient [-]
m	Mass of EV [kg]
g	Gravitational acceleration constant [m/s^2]

where μ_{rr} is the coefficient of rolling resistance. The main factors controlling μ_{rr} are the type of tire and the tire pressure. Any cyclist will know this very well; the free-wheeling performance of a bicycle becomes much better if the tires are pumped up to a high pressure, though the ride may be less comfortable. Typical values of μ_{rr} are 0.015 for a radial ply tire, down to about 0.005 for tires developed especially for electric vehicles. The rolling resistance force is primarily caused by hysteresis in the tire material when driving on a hard road surface. In figure 2.2 the pressure distribution of the contact area between the tires and the road is seen at standstill on a leveled road[14].

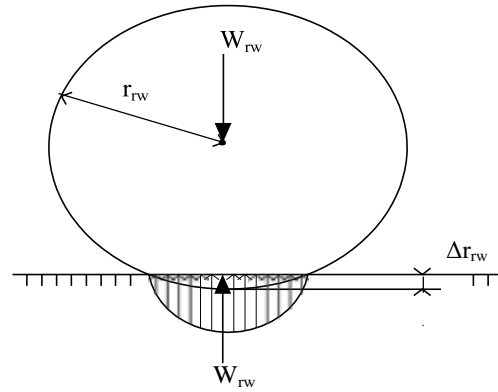


Fig 2.2: The pressure distribution of the contact area between tire and road at standstill on a leveled hard road surface

2.1.3 Aerodynamic Drag

This part of the force is due to the friction of the vehicle body moving through the air. It is a function of the frontal area, shape, protrusions such as side mirrors, ducts and air passages, spoilers, and many other factors. The formula for this component is:

$$F_{ad} = \frac{1}{2} \rho A_f C_d v^2 \quad (2.2)$$

where:	F_{ad}	Aerodynamic drag [N]
	ρ	Density of air [kg/m^3]
	A_f	Frontal area of the EV [m^2]
	C_d	Aerodynamic drag coefficient [-]
	V	Velocity of the EV [m/s]

The drag coefficient C_d can be reduced by good vehicle design. A typical value for a saloon car is 0.3, but some electric vehicle designs have achieved values as low as 0.19. There is greater opportunity for reducing C_d in electric vehicle design because there is more flexibility in the location of the major components[15].

2.1.4 Hill Climbing Force

The force needed to drive the vehicle up a slope is the most straightforward to find as shown fig 2.1. It is simply the component of the vehicle weight that acts along the slope. By simple resolution of forces, we see that:

$$F_{hc} = mg \sin(\Theta_{road}) \quad (2.3)$$

where:	F_{hc}	Hill climbing [N]
	m	Mass of EV [kg]
	g	Gravitational acceleration constant [m/s^2]
	$\sin(\Theta_{road})$	Gradient of the road

If the weight of the vehicle is assumed to be equally distributed on all four wheels, the entire rolling resistance force is found using equation (2.1) by applying the entire weight of the vehicle ($mg \sin(\Theta_{\text{road}})$) instead of just the weight on the rear wheels[11].

2.1.5 Acceleration Force

If the velocity of the vehicle is changing, then clearly a force will need to be applied in addition to the forces shown in Figure 2.1. This force will provide the linear acceleration of the vehicle, and is given by the well-known equation derived from Newton's second law,

$$F_a = ma \quad (2.4)$$

where:

F_a	Acceleration force [N]
m	Mass of EV [kg]
a	Acceleration [m/s^2]

However, for a more accurate picture of the force needed to accelerate the vehicle we should also consider the force needed to make the rotating parts turn faster. In other words, we need to consider rotational acceleration as well as linear acceleration. The main issue here is the electric motor, not necessarily because of its particularly high moment of inertia, but because of its higher angular speeds[15].

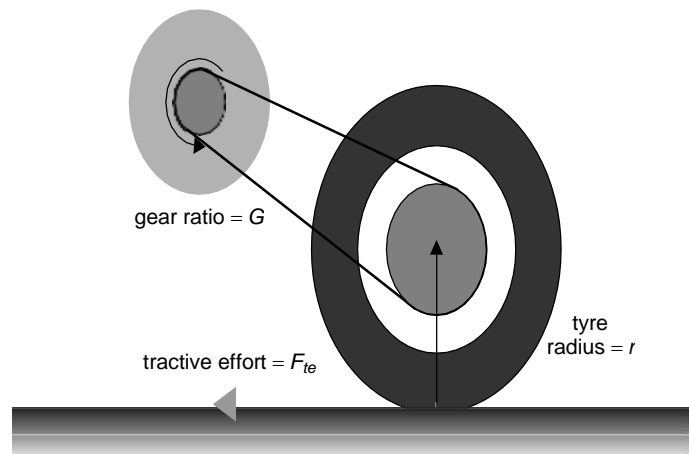


Fig 2.3: A simple arrangement for connecting a motor to a drive wheel

Referring to Figure 2.3, clearly the axle torque F_{ter} , where r is the radius of the tire, and F_{te} is the tractive effort delivered by the powertrain. If G is the gear ratio of the system connecting the motor to the axle, and T is the motor torque, the vehicle moves with angular speed then the angular acceleration is required. Angular acceleration force is the force required by the wheels to make angular acceleration ($F_{\omega a}$), as follow:

$$F_{\omega a} = I \frac{G^2}{r^2} a \quad (2.5)$$

where:

- $F_{\omega a}$ Angular acceleration force [N]
- I moment of inertia
- a Acceleration [m/s^2]
- r Radius of the tire [m]
- G Gear ratio

We must note that in these simple equations we have assumed that the gear system is 100% efficient, it causes no losses. Since the system will usually be very simple, the efficiency is often very high[16].

2.1.6 Total Tractive Effort

The total tractive effort is the sum of rolling resistance force, aerodynamic drag, hill climbing force, linear acceleration forces and angular acceleration force as follow:

$$F_t = F_{rr} + F_{ad} + F_{hc} + F_a + F_{\omega a} \quad (2.6)$$

where:

F_{rr} is the rolling resistance force, given by equation (2.1).

F_{ad} is the aerodynamic drag, given by equation (2.2).

F_{hc} is the hill climbing force, given by equation (2.3).

F_a is the force required to give linear acceleration given by equation (2.4).

$F_{\omega a}$ is the force required to give angular acceleration to the rotating motor, given by equation (2.5).

The estimated of energy is required to be determine the battery capacity according to need. The needed energy of electric vehicle is:

$$P_t = F_t \times V \quad (2.7)$$

where v is the speed of vehicle[17][18].

2.2 Modeling of Induction Motor

The proper modeling for induction machine is a key to apply the most efficient AC power supply drive to the stator windings. Mathematical modeling allows the engineer to select the best suited mathematical coordinate system transformations. These coordinate transformations are outlined in this section[19].

2.2.1 Three Phase Induction Machines

The equivalent circuit model of three phase AC machines is shown in Fig. 2.4 where the three phases of the stator and the rotor are both modeled by inductive components and appropriate AC voltage sources[20]. The stator three phase input voltages are given in equations (2.8) as well as the induced rotor three phase voltages which are given in equations (2.9).

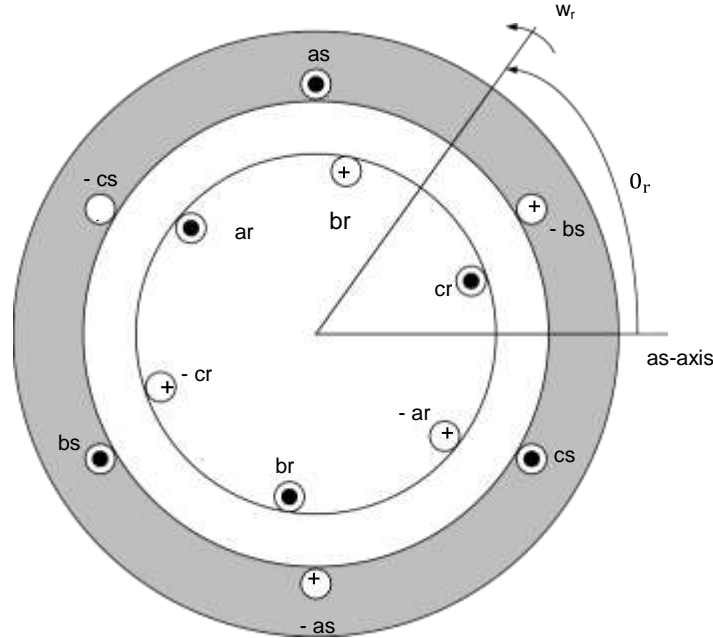


Fig 2.4: Idealized circuit model of three phase induction machine, showing the rotating stator magnetic field and the mechanically rotating rotor.

The magnetically induced stator three phase voltages in the stator coils are:

$$\begin{aligned} V_{as} &= I_{as} R_{as} + \frac{d \lambda_{as}}{dt} \\ V_{bs} &= I_{bs} R_{as} + \frac{d \lambda_{bs}}{dt} \\ V_{cs} &= I_{cs} R_{as} + \frac{d \lambda_{cs}}{dt} \end{aligned} \quad (2.8)$$

The magnetically induced rotor three phase voltages in the rotor coils are:

$$\begin{aligned} V_{ar} &= I_{ar} R_{ar} + \frac{d \lambda_{ar}}{dt} \\ V_{br} &= I_{br} R_{ar} + \frac{d \lambda_{br}}{dt} \\ V_{cr} &= I_{cr} R_{ar} + \frac{d \lambda_{cr}}{dt} \end{aligned} \quad (2.9)$$

In the above equation the s subscript denotes variables and parameters associated with the stator circuits and the r subscript denotes variable and parameters associated with the rotor circuits. The flux linkages may be expressed as

$$\begin{bmatrix} \lambda_s abc \\ \lambda_r abc \end{bmatrix} = \begin{bmatrix} L_s & L_{sr} \\ L_{sr} & L_r \end{bmatrix} \begin{bmatrix} i_s abc \\ i_r abc \end{bmatrix} \quad (2.10)$$

The winding inductance

$$L_s = \begin{bmatrix} L_{ls} + L_{ms} & -\frac{1}{2}L_{ms} & -\frac{1}{2}L_{ms} \\ -\frac{1}{2}L_{ms} & L_{ls} + L_{ms} & -\frac{1}{2}L_{ms} \\ -\frac{1}{2}L_{ms} & -\frac{1}{2}L_{ms} & L_{ls} + L_{ms} \end{bmatrix} \quad (2.11)$$

$$L_r = \begin{bmatrix} L_{lr} + L_{mr} & -\frac{1}{2}L_{mr} & -\frac{1}{2}L_{mr} \\ -\frac{1}{2}L_{mr} & L_{lr} + L_{mr} & -\frac{1}{2}L_{mr} \\ -\frac{1}{2}L_{mr} & -\frac{1}{2}L_{mr} & L_{lr} + L_{mr} \end{bmatrix} \quad (2.12)$$

$$L_{sr} = [L_{rs}]^T = L_{sr} \begin{bmatrix} \cos(\theta_r) & \cos\left(\theta_r + \frac{2\pi}{3}\right) & \cos\left(\theta_r - \frac{2\pi}{3}\right) \\ \cos\left(\theta_r - \frac{2\pi}{3}\right) & \cos(\theta_r) & \cos\left(\theta_r + \frac{2\pi}{3}\right) \\ \cos\left(\theta_r + \frac{2\pi}{3}\right) & \cos\left(\theta_r - \frac{2\pi}{3}\right) & \cos(\theta_r) \end{bmatrix} \quad (2.13)$$

In the above inductance equations, L_{ls} and L_{ms} are, respectively. The leakage and magnetizing inductance of the stator winding; L_{lr} and L_{mr} are for the rotor winding. The inductance L_{sr} is the amplitude of the mutual inductance between stator and rotor windings.

The three-phase induction machine is therefore, represented in circuit form by employing the six independent and distinct stator and rotor equations in (2.8) and (2.9), respectively. The flux linkage that enters into the air gap region, has two parts and the mutual inductance between the rotor and stator is depending on the rotor position, so it is depended on the rotor angle (θ_r). That means the rotor and stator equations are depending on each other (mutual coupling). To make the dynamic IM model easier, clever mathematical transformations or mappings between coordinate systems are used, which is explained in the next section[21].

2.2.2 Machine Model in Arbitrary Reference Frames

There are three main reference frames of motion, which could be used to model the three-phase induction machine in its three main regions of operation. These are the stationary reference frame for startup, the synchronous reference frame for equilibrium motion, and the rotor reference frame for changing speeds by acceleration or deceleration. The two commonly employed coordinate transformations with induction machine are the stationary and the synchronous reference frame. These mathematical transformations, which are known as Park Transformation [22], can facilitate understanding of the variation of the mutual inductance between the stator and the rotor under differing rotation conditions[20].

Referring to Fig. 2.5 and deriving the equations for three phase induction machines in arbitrary reference frame with the speed w_r in the same direction of rotor rotation. This arbitrary frame can then be specified as stationary or synchronous. When $w = 0$, this means the reference frame does not move (stationary) and this transformation is commonly used in Adjustable Speed Drives. Similarly, when the reference frame is revolving in the synchronous speed, the reference frame can be represented in synchronous reference frame. This is a representation used to simulate power system components. By applying rotating coordinate transformations to the stator and rotor voltages, current and flux linkage equations, which are represented in equations (2.8) -(2.13) respectively, those equations can be represented in simpler form by proper choice of reference frames[23].

$$\begin{bmatrix} f_q \\ f_d \\ f_0 \end{bmatrix} = T_{qdo}(\theta) \begin{bmatrix} f_a \\ f_b \\ f_c \end{bmatrix} \quad (2.14)$$

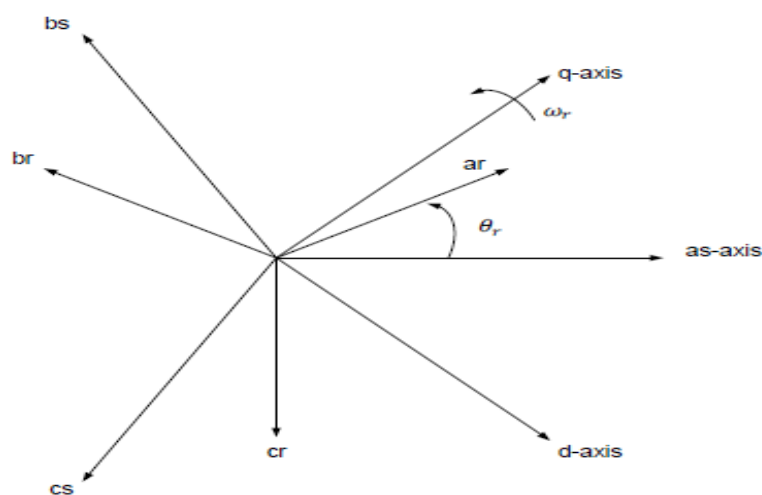


Fig 2.5: Relationship between ABC and qdo arbitrary coordinate reference frames.

Where f can be stator or rotor voltage, current as well as a flux linkage of the stator or rotor of the induction machine, located in the air gap region between stator and rotor. $T_{qdo}(\theta)$ is the associated torque transformation matrix.

$$T_{qdo}(\theta) = \frac{2}{3} \begin{bmatrix} \cos(\theta) & \cos\left(\theta - \frac{2\pi}{3}\right) & \cos\left(\theta + \frac{2\pi}{3}\right) \\ \sin(\theta) & \sin\left(\theta - \frac{2\pi}{3}\right) & \sin\left(\theta + \frac{2\pi}{3}\right) \\ \frac{1}{2} & \frac{1}{2} & \frac{1}{2} \end{bmatrix} \quad (2.15)$$

The inverse of the transformation matrix obtained by matrix methods is:

$$[T_{qdo}(\theta)]^{-1} = \begin{bmatrix} \cos(\theta) & \sin(\theta) & 1 \\ \cos\left(\theta - \frac{2\pi}{3}\right) & \sin\left(\theta - \frac{2\pi}{3}\right) & 1 \\ \cos\left(\theta + \frac{2\pi}{3}\right) & \sin\left(\theta + \frac{2\pi}{3}\right) & 1 \end{bmatrix} \quad (2.16)$$

2.2.2.1 The qdo stationary reference frame equations applicable for motor start up conditions

In summary we list below the various voltages in the stator and rotor as well as the flux linkages which determine the various shaft torques in the " stationary qdo reference frame".

$$\begin{aligned} v_{qs}^s &= \frac{p}{w_b} \psi_{qs}^s + R_s i_{qs}^s \\ v_{ds}^s &= \frac{p}{w_b} \psi_{ds}^s + R_s i_{ds}^s \\ v_{os} &= \frac{p}{w_b} \psi_{os} + R_s i_{os} \\ v_{qr}^s &= \frac{p}{w_b} \psi_{qr}^s - \frac{w_r}{w_b} \psi_{dr}^s + R_r' i_{qr}^s \\ v_{dr}^s &= \frac{p}{w_b} \psi_{dr}^s - \frac{w_r}{w_b} \psi_{qr}^s + R_r' i_{dr}^s \\ v_{or} &= \frac{p}{w_b} \psi_{or}' + R_r' i_{or}' \end{aligned} \quad (2.17)$$

Flux linkage equations in Matrix Notification

$$\begin{bmatrix} \Psi_{qs}^s \\ \Psi_{ds}^s \\ \Psi_{os}^s \\ \Psi_{dr}^s \\ \Psi_{qr}^s \\ \Psi_{or}^s \end{bmatrix} = \begin{bmatrix} x_{Ls} + x_m & 0 & 0 & x_m & 0 & 0 \\ 0 & x_{Ls} + x_m & 0 & 0 & 0 & 0 \\ 0 & 0 & x_{Ls} & 0 & 0 & 0 \\ x_m & 0 & 0 & x'_{lr} + x_m & 0 & 0 \\ 0 & x_m & 0 & 0 & x'_{lr} + x_m & 0 \\ 0 & 0 & 0 & 0 & 0 & x'_{lr} \end{bmatrix} \begin{bmatrix} i_{qs}^s \\ i_{ds}^s \\ i_{os}^s \\ i_{qr}^s \\ i_{dr}^s \\ i_{or}^s \end{bmatrix} \quad (2.18)$$

The torque Equations is given as follows

$$\begin{aligned} T_{em} &= \frac{3}{2} \frac{p}{2} \frac{1}{w_b} (\Psi_{qr}^s i_{dr}^s - \Psi_{dr}^s i_{qr}^s) \text{ N.M} \\ T_{em} &= \frac{3}{2} \frac{p}{2} \frac{1}{w_b} (\Psi_{ds}^s i_{qs}^s - \Psi_{qs}^s i_{ds}^s) \text{ N.M} \\ T_{em} &= \frac{3}{2} \frac{p}{2} \frac{1}{w_b} x_m (i_{qs}^s i_{dr}^s - i_{ds}^s i_{qr}^s) \text{ N.M} \end{aligned} \quad (2.19)$$

2.2.2.2 The qdo synchronous reference frame equations applicable for near synchronous equilibrium motor operation

For comparison we list below the various voltages in the stator and rotor as well as the flux linkages which determine the various shaft torques in the "synchronous rotating qdo rotating reference frame".

$$\begin{aligned} v_{qs}^e &= \frac{p}{w_b} \Psi_{qs}^e + \frac{w_e}{w_b} \Psi_{qs}^e + R_s i_{qs}^e \\ v_{ds}^e &= \frac{p}{w_b} \Psi_{ds}^e + \frac{p}{w_b} \Psi_{ds}^e + R_s i_{ds}^e \\ v_{os} &= \frac{p}{w_b} \Psi_{os} + R_s i_{os} \\ v_{qr}^e &= \frac{p}{w_b} \Psi_{qr}^e - \frac{w_e - w_r}{w_b} \Psi_{dr}^e + R'_r i_{qr}^e \\ v_{dr}^e &= \frac{p}{w_b} \Psi_{dr}^e - \frac{w_e - w_r}{w_b} \Psi_{qr}^e + R'_r i_{dr}^e \\ v'_{or} &= \frac{p}{w_b} \Psi'_{or} + R'_r i'_{or} \end{aligned} \quad (2.20)$$

Flux linkage equations in Matrix Notification

$$\begin{bmatrix} \Psi_{qs}^e \\ \Psi_{ds}^e \\ \Psi_{os} \\ \Psi_{dr}^e \\ \Psi_{qr}^e \\ \Psi_{or}^e \end{bmatrix} = \begin{bmatrix} x_{Ls} + x_m & 0 & 0 & x_m & 0 & 0 \\ 0 & x_{Ls} + x_m & 0 & 0 & x_m & 0 \\ 0 & 0 & x_{Ls} & 0 & 0 & 0 \\ x_m & 0 & 0 & x'_{lr} + x_m & 0 & 0 \\ 0 & x_m & 0 & 0 & x'_{lr} + x_m & 0 \\ 0 & 0 & 0 & 0 & 0 & x'_{lr} \end{bmatrix} \begin{bmatrix} i_{qs}^e \\ i_{ds}^e \\ i_{os} \\ i_{qr}^e \\ i_{dr}^e \\ i_{or}^e \end{bmatrix} \quad (2.21)$$

The torque Equations is given as follows

$$\begin{aligned} T_{em} &= \frac{3}{2} \frac{p}{2} \frac{1}{w_b} (\Psi_{qr}^e i_{dr}^e - \Psi_{dr}^e i_{qr}^e) \text{ N.M} \\ T_{em} &= \frac{3}{2} \frac{p}{2} \frac{1}{w_b} (\Psi_{ds}^e i_{qs}^e - \Psi_{qs}^e i_{ds}^e) \text{ N.M} \\ T_{em} &= \frac{3}{2} \frac{p}{2} \frac{1}{w_b} x_m (i_{qs}^e i_{dr}^e - i_{ds}^s i_{qr}^e) \text{ N.M} \end{aligned} \quad (2.22)$$

It can be noticed that the equations (2.17)- (2.22), which represent the differential equations for the dynamic simulation for three phase induction machines transformed to stationary and synchronous reference frames, have the term ψ which is simply the multiplication of the flux linkage λ by the rated angular speed w_b .

$$\psi = w_b \lambda \quad (2.23)$$

$$x = w_b L \quad (2.24)$$

There is also the superscript s to indicate that the equation is represented in stationary reference frame and the superscript e for the synchronous reference frame[24].

2.3 Analysis of Various Methods for Speed Control of Induction Motor

The various methods of speed control of 3 – ϕ induction motor are as the following [24]:

1. Pole Changing.
2. Variable Supply Voltage Control.
3. Variable Rotor Resistance Control.
4. Variable Supply Frequency Control.
5. Constant V/F control.
6. Slip Recovery.
7. Vector Control.

However, we shall not be analyzing the pole changing and the variable supply frequency methods as these are very rarely used. Also slip recovery and vector control shall not be analyzing.

2.3.1 Variable Rotor Resistance

This method is applicable only to the wound rotor motor as external resistance can be added to it through the slip rings. The torque-speed characteristics are shown in Fig. 2.6 below.

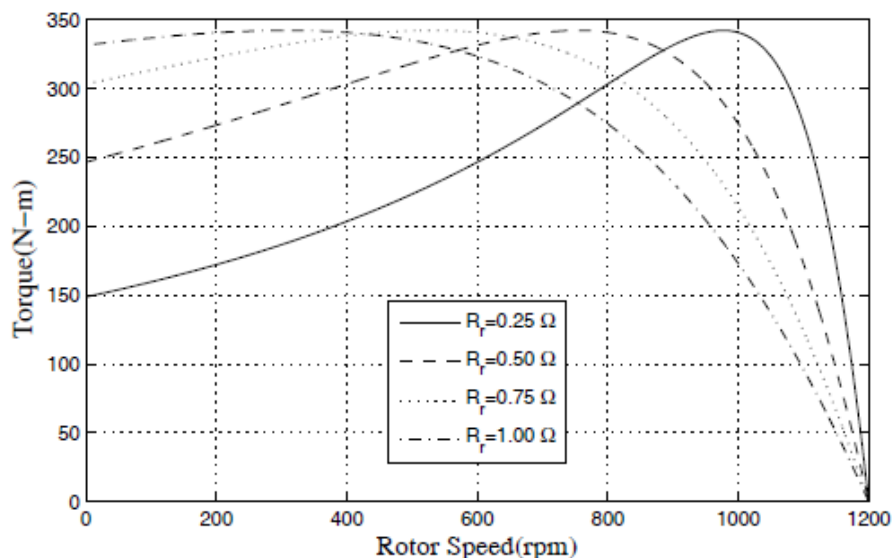


Fig 2.6: Torque-speed characteristics of a 3 – ϕ IM with variable rotor resistance.

External resistances can be connected in the rotor circuit during starting. This increases the starting torque and reduces the starting current. By making use of appropriate value of resistors, the maximum torque can be made to appear during starting. This can be used in applications requiring high starting torque. Once the motor is started, the external resistance can be cut out to obtain high torque throughout the accelerating range. As external resistances are connected, most of the I^2R loss is dissipated through them thus the rotor temperature rise during starting is limited.

2.3.2 Variable Stator Voltage

The torque developed by an IM varies as square of the voltage applied to its stator terminals. Thus, by varying the applied voltage, the electromagnetic torque developed by the motor can be varied. This method is generally used for small squirrel-cage motors where cost is an important criterion and efficiency is not. However, this method has rather limited range of speed control. The torque-speed characteristics are shown in Fig. 2.7 below.

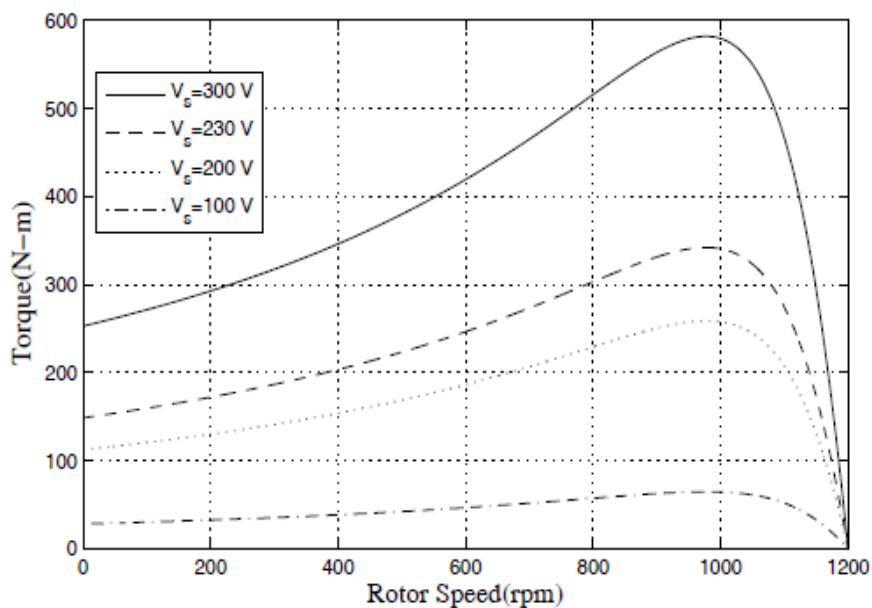


Fig 2.7: Torque-speed characteristics of a 3 – ϕ IM with variable stator voltage.

As the supply voltage is decreased, the value of maximum torque also decreases, However, it still occurs at the same slip as earlier. Even the starting torque and the overall torque reduce. Therefore the machine is highly underutilized. Therefore this method of speed control has very limited applications.

2.3.3 Constant V/F Control

We vary the stator voltage in such a way that the flux remains constant by simultaneously varying the supply frequency in such a way that the ratio V/f remains constant. The torque-speed characteristics are shown in Fig. 2.8 below.

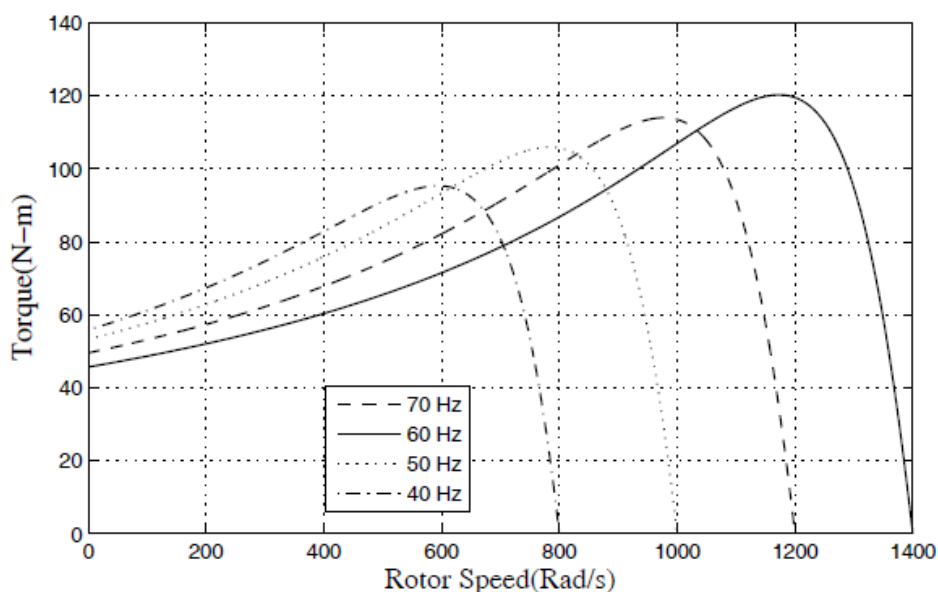


Fig 2.8: Torque-speed characteristics of a 3 – ϕ IM with constant V/F method.

At the base speed, the voltage and frequency reach the rated values. We can drive the motor beyond the base speed by increasing the frequency further. However, the applied voltage cannot be increased beyond the rated voltage. Therefore, only the frequency can be increased, which results in the reduction of torque. Above the speed the factors governing torque become complex. The IM draws the rated current and delivers the rated torque at the base speed.

When the load is increased, while running at base speed, the speed drops and slip increases. The motor can take up to 2.5 times rated torque with around 20% drop in speed. Any further increase of load on the shaft can stall the motor. The torque developed by the motor is directly proportional to the magnetic field produced by the stator. So, the voltage applied to the stator is directly proportional to the product of the stator flux and angular velocity. This makes the flux produced by the stator proportional to the ratio of applied voltage and frequency of supply. By varying the frequency, the speed of the motor can be varied. Therefore, by varying the voltage and frequency by the same ratio, flux and hence the torque can be kept constant throughout the speed range. This makes constant V/f the most common speed control of the IM. The equations (2.25) and (2.26) shows the relationship between the voltage and torque versus frequency.

$$V = \phi 2\pi f \quad (2.25)$$

$$\phi = \frac{V}{f} \quad (2.26)$$

The voltage and frequency being increased up to the base speed. At the base speed, the voltage and frequency reach the rated values. We can drive the motor beyond base speed by increasing the frequency further. However, the voltage applied cannot be increased the rated voltage. Therefore, only the frequency can be increased, which results in the field weakening and torque available is being reduced. Above base speed, the factors governing torque become complex, since friction and windage losses increase significantly at highest speeds. Hence, the torque curve becomes nonlinear with respect to speed or frequency[25].

2.2 Electric Vehicle impacts and performance

There is clearly a wide range of input parameters that can be used for the models, and there is an equally wide range of output variables that the models can measure. The model outputs can be broadly categorized as economic, environmental, grid performance, and renewable energy-related. Some key findings for the first three categories of outputs will be briefly discussed in this section before a more thorough and comprehensive review of studies that focused on the integration of renewable energy into the electricity system is conducted[26].

2.4.1 Economic Impacts

The economic impacts of EVs are generally examined from two perspectives: that of a vehicle owner, and that of the electricity system. The lifecycle economics of EVs are expected to improve with better battery technology and mass production. Currently, BEVs cost more than traditional ICEVs[27]. However, the fuel and operating costs of EVs are much lower than ICEVs, due to the high efficiency of an electric motor. estimate that the payback time for a BEV, in comparison to a cheaper ICEV, is currently 20 years, but it should drop to less than five years by 2030. estimate that the total lifetime costs of ownership for all vehicle types will converge by 2030[28].

2.4.2 Environmental Impacts

CO₂ emissions are the most commonly measured output used to assess the environmental impacts of switching to EVs[29]. find that the use of EVs decreases CO₂ emissions compared to ICEVs even if there is no wind energy present in the generation mix. There is debate over what emissions intensity (CO₂e/kWh) should be assigned to the electricity used by electric vehicles when charging. Most studies use the average grid intensity to reflect a situation in which EVs are widely adopted and should be considered as part of the everyday demand profile, in which the emissions of the marginal generating unit are assigned to EV electricity. In most markets, especially at times of peak demand, this will be a natural gas or coal power plant which will lead to larger carbon emissions from EVs. However, even studies that utilize the marginal mix in different regions find a net carbon benefit in comparison to the use of ICEVs[30]. In general, it can be seen that EVs reduce total CO₂ emissions even in electricity systems with a high fraction of fossil fuel generation, due to the high efficiency of an electric motor in comparison to an internal combustion engine[31].

2.4.3 Grid Impacts

Electric vehicles affect the performance, efficiency, and required capacity of the electric grid, especially if vehicle charging is unconstrained. The found that peak loads will increase under a simple charging strategy, requiring extra investment in generation and transmission capacity. When the vehicles use a smart charging plan, studies indicate that EVs levelized the overall load, make better use of baseload units, and require no extra installed capacity[32]. Other impacts of EVs on the distribution grid include increased wear on transformers, transmission bottlenecks and power quality issues; these and other more technical issues are thoroughly reviewed. There are conflicting findings on the effect of EVs on distribution networks. They suggest that network reinforcements, embedded generation and EV charge management strategies are needed to safely integrate large numbers of EVs into distribution networks [33].

2.5 Vehicles and Energy Source

An electric vehicle will be defined, as any vehicle in which some or all of the driving energy is supplied through electricity from a battery. In a conventional internal combustion engine vehicle (ICEV), gasoline or diesel fuel is combusted to create mechanical energy that provides the power to move the vehicle forward. A number of EV technologies are currently in use or under development [34]. A hybrid electric vehicle (HEV) has a small electric battery that supplies electricity to the drivetrain in order to optimize the operating efficiency of the combustion engine. The battery in an HEV can be charged by the engine or through captured kinetic braking energy from a process called regenerative braking. HEVs are more fuel efficient than ICEVs, but ultimately the vehicle is fully powered by liquid fuels. A plug-in hybrid electric vehicle (PHEV) is similar in concept to an HEV, but with a larger battery and a grid connection. The grid connection allows the battery to be charged with electricity and the larger battery size enables the car to drive a significant distance in all- electric mode. A battery electric vehicle (BEV) is fully powered by grid electricity stored in a large onboard battery. EVs use energy much more efficiently than ICEVs; a traditional ICEV fuel efficiency is 15–18%, while a BEV can be as high as 60–70% efficient. The battery of an electric vehicle can be recharged from the grid with varying measures of external control, labeled here as charge plans. A simple, or unconstrained, charge plan is a system in which the vehicle immediately begins recharging as soon as it is connected to the grid. A delayed charge plan offsets the battery charging by a set amount of time, for example three hours. Nighttime charge plans delay charging to occur over the course of the night when electricity prices are lowest, with the battery fully charged for use in the morning[35].

2.5.1 Solar Energy

The literature on solar energy and EVs is much more diverse than the previously reviewed studies that integrate PV system and batteries vehicles. Electricity from solar PV can be produced anywhere; this provides more interesting methods to directly integrate energy production and use in EVs. A few representative studies of these varying approaches are discussed [35].

2.5.2 Battery for Electric Vehicle

The high voltage battery is the main power source for the electric motor drive. The battery is sized in its capacity to provide enough energy to last a typical drive period in a day. However, depending on the road conditions and the gradients encountered, the charge may not last that long. Hence, a need to re-charging the battery during the day may arise. It is critical for the control system to operate the vehicle and the motor drive system in the most efficient way possible to ensure highest mileage per battery charge. Rechargeable battery technology involves chemistry and physics. Lithium Ion type battery has emerged as the leading type in most portable devices. However, for

larger systems like the vehicles, Li-ion is also desirable due to its relatively high energy density. An Wh/Kg for various battery types is shown in Fig 2.9 for comparison purposes[36].

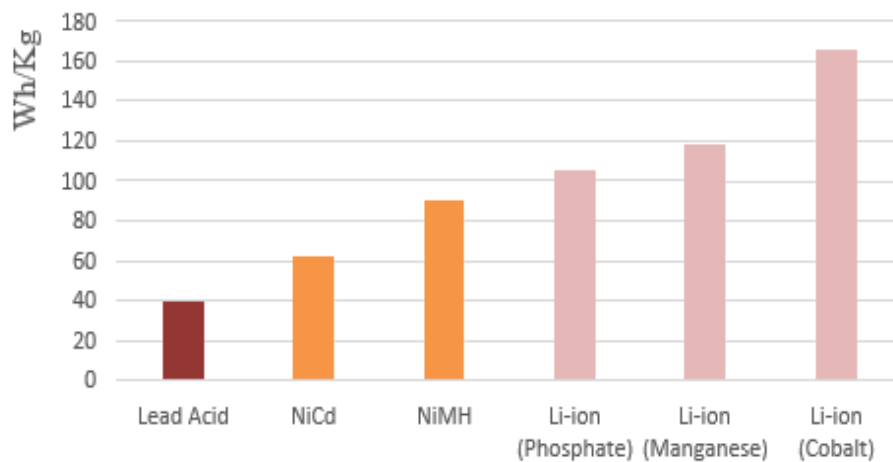


Fig 2.9: Wh/Kg for various battery types.

The fuel economy and all-electric range (AER) of hybrid electric vehicles (HEVs) are highly dependent on the on-board energy-storage system (ESS) of the vehicle. Energy-storage devices charge during low power demands and discharge during high power demands, acting as catalysts to provide energy boost. Batteries are the primary energy-storage devices in ground vehicles[37].

2.5.2.1 Lead–Acid Batteries

The spongy lead works as the negative active material of the battery, lead oxide is the positive active material, and diluted sulfuric acid is the electrolyte. For discharging, both positive and negative materials are transformed into lead sulfate[38]. The lead–acid battery presents several advantages for HEV applications. They are available in production volumes today, yielding a comparatively low-cost power source. In addition, lead–acid battery technology is a mature technique due to its wide use over the past 50 years. However, the lead–acid battery is not suitable for discharges over 20% of its rated capacity. When operated at a deep rate of state of charge (SOC), the battery would have a limited life cycle. The energy and power density of the battery is low due to the weight of lead collectors. Research efforts have found that energy density can be improved by using lighter noncorrosive collectors [36]

2.5.2.2 Lithium-Ion Batteries

The lithium-ion battery has been proven to have excellent performance in portable electronics and medical devices [39]. The lithium-ion battery has high energy density, has good high- temperature performance, and is recyclable. The positive electrode is made of an oxidized cobalt material, and

the negative electrode is made of a carbon material. The lithium salt in an organic solvent is used as the electrolyte. The promising aspects of the Li-ion batteries include low memory effect, high specific power of 300 W/kg, high specific energy of 100 Wh/kg, and long battery life of 1000 cycles. These excellent characteristics give the lithium-ion battery a high possibility of replacing NiMH as next-generation batteries for vehicles[40].

2.5.2.3 Nickel–Cadmium (Ni–Cd) Batteries

Nickel–cadmium batteries have a long lifetime and can be fully discharged without damage. The specific energy of Ni–Cd batteries is around 55 Wh/kg. These batteries can be recycled, but cadmium is a kind of heavy metal that could cause environmental pollution if not properly disposed of. Another drawback of Ni–Cd batteries is the cost[41], [42].

2.6 conclusion

It introduces mechanical analysis of an EV is presented to determine the forces acting on it when driving and modeling of three phase induction motor, based on battery is sized in its capacity to provide enough energy to last a typical drive period in a day. It is critical for the control system to operate the vehicle and the motor drive system in the most efficient way possible to ensure highest mileage per battery charge. Rechargeable battery technology involves chemistry and physics. The lead–acid battery presents several advantages for HEV applications. Nickel–cadmium batteries have a long lifetime and can be fully discharged without damage. The lithium-ion battery has been proven to have excellent performance in HEV applications and medical devices.

Performance Comparison of Fuzzy Logic and PI Controllers Based on MPPT Algorithms for PV systems

3.1 Introduction

Generation of electricity from photovoltaic has obtained worldwide acceptance due to its eco-friendly nature and abundant availability. This availability is subjected to variation owing to many factors such as in shadow, irradiation, temperature etc. Therefore, practical measurements of atmospheric temperature and solar irradiation change are made over several days. This paper presents evaluation for different control techniques among the most usual maximum power point tracking (MPPT) algorithms. The compares the performance between fuzzy logic and PI controllers with P&O algorithm. This comparison will be made with respect to the amount of energy extracted from photovoltaic (PV), using MATLAB/SIMULINK, dynamic response, and use of sensors. In the experimental setup, a digitally controlled boost DC-DC converter based on P&O algorithm for fuzzy logic and PI controllers, is used to generate PWM pulses for the switches. The main experimental results show the effect of solar irradiation and temperature for conventional MPPT algorithms and improved MPPT algorithm using P&O with fuzzy logic controller[8]. The fuzzy logic controller has merits of its accuracy, reliability, faster dynamic response, and ability to track the global peak power accurately under change in environmental conditions with almost zero steady state oscillations. The growing energy demand is coupled with the possibility of lower supply of conventional fuels. Moreover, with growing concerns about environmental conservation, the electrical energy from solar (PV) cells is currently regarded as a natural energy source that is more useful. This is due to that it is free, abundant, clean, distributed over the Earth, and contribute as a primary factor of all other processes of energy production. The used MPPT techniques are important to extract the maximum power available in solar PV. Therefore, the operating current and voltage which maximize power output will be varied with environmental conditions [7], [9].

The perturbation and observation P&O, the IC methods based on fixed iteration step size are simple and have good performances. Therefore, they are characterized by slow convergence, oscillations in the PV power around the MPP, operation failure under rapidly changing atmospheric temperature, and irradiation conditions. Using small perturbation step size will result in reduced oscillations, but the speed of tracking MPPT remains slower. To acquire a fast response speed and to overcome the aforementioned drawbacks, a modified MPPT algorithms with variable step size have been the subject of many investigations. Generally, the conventional (IC) MPPT algorithm uses a fixed step size and oscillation can be reduced to track the (MPP) [43], [44].

3.2 Modeling of Photovoltaic Cell

Solar cell is an electrical device that converts the light energy into electricity by the photovoltaic effect. In ideal PV cell, the efficiency of solar cells depends on many factors, such as the solar irradiation, the temperature, the spectral characteristics of sunlight, shaded condition, the dirt, and the output voltage of the PV module, etc. The simplest equivalent PV panel can be modeled as a current source in parallel with a diode, shunt resistance R_{sh} and a series resistance R_s as shown in Fig. 3.1. To increase the output power of the system, PV modules are generally made up using several PV cells connected in series and/or in parallel[45].

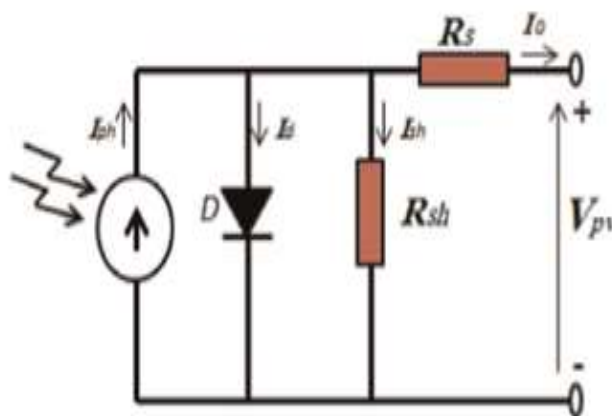


Fig 3.1: Equivalent Simplified circuit of a photovoltaic cell.

When PV cell is supplied solar irradiance the output current from the solar PV cell can be found using Kirchhoff's law, Based on Fig. 3.1 the output current of the solar cell can be given by, as shown in Eq. (3.1):

$$I_o = I_{ph} - I_d - I_{sh} \quad (3.1)$$

where: I_{ph} is the current generated by the incident light (it is directly proportional to the Sun irradiation).

I_d is the current through the diode.

I_{sh} is the current through the parallel resistor R_{sh} .

where I_{ph} is the light generated current in PV cell and given as in Eq. (3.2):

$$I_{ph} = G \{I_{sc} [1 + a (T - T_{STC})]\} \quad (3.2)$$

Where:

- G is the solar irradiance.
- I_{sc} is the PV short circuit current
- a is the temperature coefficient of short circuit current
- T is the temperature operation.
- T_{STC} is the temperature operation for the PV cell under standard test conditions (STC).

And I_d is the diode current and given as Eq. (3.3):

$$I_d = I_{rs} \left[\exp\left(\frac{qV_d}{\eta kT}\right) - 1 \right] \quad (3.3)$$

where

- I_{rs} is the reverse saturation current of the diode
- V_d is the Voltage across diode
- q is the electric charge (1.69×10^{-19} C).
- k is the Boltzmann's constant (1.38×10^{-23} J/ K).
- η is the diode idealist factor?

The PV panel simulation model is based on the output current of one PV equivalent model, and its mathematical equation is represented given as Eq. (3.4)

$$I_o = I_{Ph} - I_{rs} \cdot \left[e^{q \cdot (V + I \cdot R_s) / \eta \cdot k \cdot T} - 1 \right] - \frac{V + I \cdot R_s}{R_{sh}} \quad (3.4)$$

Where

- V is the represents the output PV voltage of one PV panel
- I_{Ph} is the photocurrent
- I_{rs} is the reverse saturation current of the diode
- q is the electrical charge (1.6×10^{-19} C)
- η is the p-n junction quality factor
- k is the Boltzmann constant (1.38×10^{-23} J/K)
- T is the temperature (in kelvins).

where I_o is the PV output current, and V is the PV output voltage of PV cell. Solar cells are connected in parallel and series to obtain desired current and voltage respectively for the solar panel, and then the solar panels are connected in series and/or parallel to give different configurations of PV array[46], [47].

Table 3.1: Electrical parameter of the PV module

SYMBOL	DISCRETION	QUANTITY
P_{max}	Maximum power	250 Watt
V_{mpp}	Voltage at MPP	29.65 V
I_{mpp}	Current at MPP	8.47 A
V_{oc}	Open circuit voltage	37.22 V
I_{sc}	Short circuit current	8.51 A
α	Temperature coefficient of I_{sc}	$3.18 \times 10^{-3} \text{ A/C}^\circ$

the PV cell which are given from a typical PV panel MATLAB/SIMULINK and experimental results. The electrical parameters are listed in Table 3.1.

3.3 Effects of PV Solar on MPP

However, the MPP of a PV panel is not fixed but varies with different factors such as solar irradiance and temperature. In the following sections, we describe the variation of MPP with different irradiance and temperature[48].



Fig. 3.2 a: as shown the measurement devices such as solar radiation, temperature measurement, variable resistance, and PV module

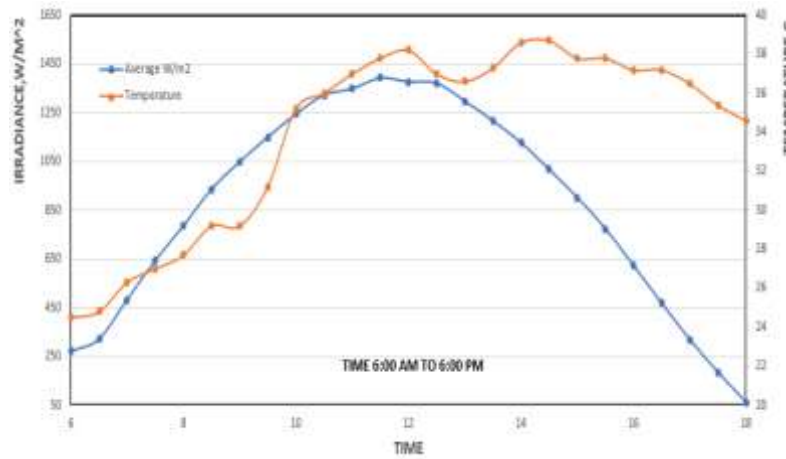


Fig. 3.3: Experimental results of variation of irradiation and temperatures from 6 am to 6 pm in Sohag city



Fig. 3.2 b: Experimental prototype using PV solar of electric vehicle.

Experimental measurement devices as shown fig 3.2 a. readings for variation of various irradiation and temperatures from 6 am to 6 pm in Sohag city, are shown in Fig 3.3. The curves show clearly the nonlinear characteristics that are strongly influenced by climate changes.

3.3.1 Effects of Solar Irradiance on MPP

There are two key parameters frequently used to characterize a PV cell. Shorting together the terminals of the cell, the photon generated current will follow out of the cell as a short-circuit current (I_{sc}). When there is no connection to the PV cell (open-circuit), the photon generated current is shunted internally by the intrinsic p-n junction diode. This gives the open circuit voltage (V_{oc}). The PV module or cell manufacturers usually provide the values of these parameters in their datasheet as shown table 3.1. In a PV cell current is generated by photons and output is constant under constant temperature and constant incident radiation of light. Varying the irradiation, we can get different output levels[49].

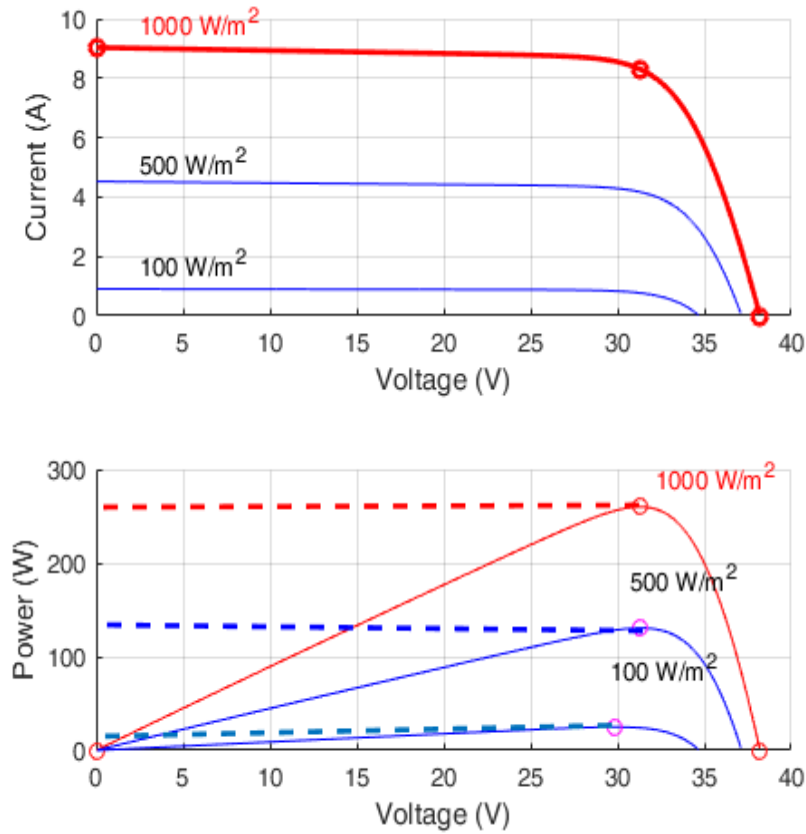


Fig. 3.4: I-V and P-V curves of the PV module under various values of irradiation (100, 500, 1000 W/m²).

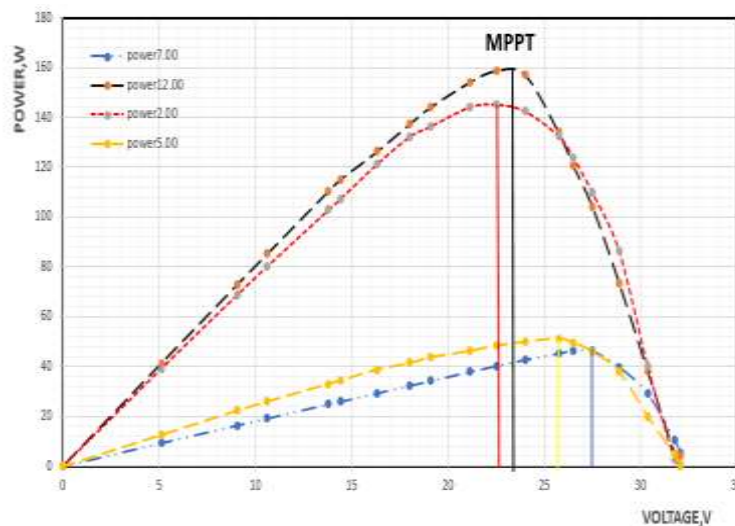


Fig. 3.5: Experimental results of variation of irradiation and temperatures from 6 am to 6 pm P-V power characteristic for different irradiation and temperature levels in Sohag city fig (c).

The PV cell output is both limited by the cell current and the cell voltage, and it can only produce a power with any combinations of current and voltage on the I-V curve. As in Fig 3.4. the P-V curve shifts with different irradiance and temperature as in Fig 3.5. Experimental results in Sohag

city so the MPP also shifts. Now, as the I-V curve of a PV cell changes with different irradiance so it reveals that the amount of power produced by the PV module varies greatly depending on its irradiance. It is important to operate the system at the MPP of PV module in order to exploit the maximum power from the module[50].

3.3.2 Effects of temperature on MPP

I-V characteristic of a PV module varies at various module temperatures. With the increase of temperature, the I-V characteristics of a PV cell shifts toward lefts and so the MPP decreases with increase in temperature as shown fig 3.6.

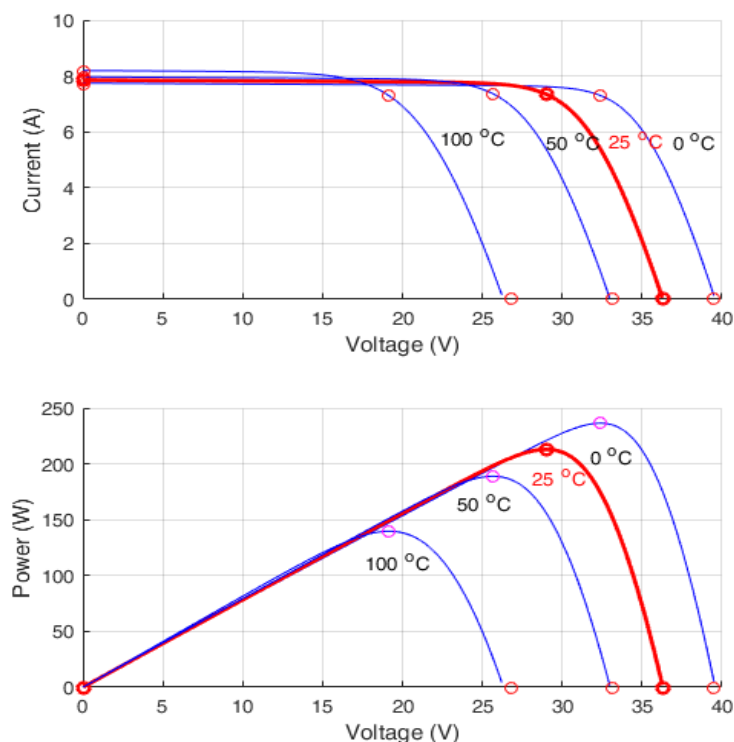


Fig. 3.6: IV and PV curves of the PV module under various values of temperature (0, 25, 50, 100 C°)

Because of the photovoltaic nature of solar panels, their current-voltage, or IV, curves depend on temperature and irradiance levels. Therefore, the operating current and voltage which maximize power output will change with environmental conditions. Therefore, the MPP needs to be located by a tracking algorithm, which is the heart of MPPT controller. MPPT algorithm tells controller how to move the operating voltage. Then, it is a MPPT controller's task to bring the voltage to a desired level and maintain it. To obtain a stable voltage from an input supply (PV cells) that is higher and lower than the output, a high efficiency and minimum ripple DC-DC converter required in the system[51].

3.4 Maximum Power Point Tracking

For any given set of operational conditions, cells have a single operating point where the values of the current (I) and voltage (V) of the cell result in a maximum power output. These values correspond to a particular load resistance, $R = V/I$, as specified by Ohm's Law. The power P is given by $P = V \cdot I$. From basic circuit theory, the power delivered from or to a device is optimized where the derivative of the I-V curve is equal and opposite the I/V ratio. There is a unique point on the P-V curve of a PV array called the (MPP), with its location shifting according to weather conditions. The MPPT technique, in general, the MPPT is an electronic system, the principle of which is to feed the appropriate duty cycle (D). This is a dynamic quantity which changes depending on the level of illumination, as well as other factors such as temperature and the age of the cell. If the resistance is lower or higher than this value, the power drawn will be less than the maximum available, and thus the cell will not be used as efficiently as it could be. Maximum power point trackers utilize different types of control circuit or logic to search for this point and thus to allow the converter circuit to extract the maximum power available from a cell[51], [52].

3.4.1 Power Conversion System

To improve the stability, reliability and quality of the output of PV system generation, a power conversion system is employed [9]. There are two types for PV power conversion; single stage and double stage power conversion, Although the single stage-power conversion system is lower in cost due to its fewer part count, it suffers from several drawbacks such as hot-spots during partial shading conditions of the PV array and reduced safety. Those issues occurred in grid-connected PV system due to a large change in DC voltage of PV array. Therefore, the first stage is used to boost the MPP voltage and the second stage converts this DC power into high quality AC power. In first stage, a DC-DC boost converter is widely used for the PV generated system due to its high efficiency and easily adapted MPPT controller. It is used to provide and regulate an appropriate the output voltage that has level which is considerably more than the input voltage, converter is a transistor [IGPT or MOSFET], which regulates the amplified processing by a controller. The MOSFET transistor is usually used for this kind of converter, the voltage gain of the circuit (boost) is given as in Eq. (3.5) [51]:

$$G_n = \frac{v_o}{v_i} = \frac{1}{1-D} \quad (3.5)$$

Where V_o = output voltage, V_i = input voltage, and D = duty cycle of DC-DC boost converter, which is converted to a control signal by a gate driver circuit. The principle work of this converter divides into two states, first, when the MOSFET is switched ON; the current flows through an inductor (L) in a reverse direction and the inductor stores the energy by generating a magnetic field, while the output capacitor (C2) transfers its energy to the load or inverter. In state two, when

the transistor is switched OFF, the energy stored and main source will be in series, which leads to a higher output voltage. In the grid-connected PV system, the DC-DC boost converter plays a crucial role in maintaining a constant DC voltage system for a DC-AC inverter[53].

3.5 Methods of MPPT Algorithms

Maximum Power Point Tracking (MPPT) is used to obtain the maximum power from these systems. In these applications, the load can demand more power than the PV system can deliver. There are many different approaches to maximizing the power from a PV system, this range from using simple voltage relationships to more complex multiple sample-based analysis[5].

There are some conventional methods for MPPT. Seven of them are listed here. These methods include:

1. Constant Voltage method
2. Open Circuit Voltage method
3. Short Circuit Current method
4. Perturb and Observe method
5. Incremental Conductance method
6. Temperature method
7. Temperature Parametric method

the demonstrates that the performance of the classical P&O method under sudden changes of irradiation is different from that under sudden variation of ambient temperature, so it is very significant to track the (MPP) for an effective PV system. So, in PV systems a (MPPT) is extremely needed. In generality PV systems a control algorithm, namely (MPPT)algorithm is utilized to have the full characteristic of the PV systems. Improvements can be obtained through a digital controller, transforming the conventional P&O into an adaptive solution once different step sizes according to the tracking of the MPP are performed[5].

3.5.1 Perturb and Observe Method

The P&O algorithm is widely used for PV-MPPT due to its low cost and simple implementation, the principle work of this algorithm calculating the PV power by using the sensed values of the voltage and current of the PV module[12]. These are then compared with the previous power and voltage, with the direction of the algorithm being adjusted accordingly and the duty cycle of the boost converter being adjusted as in Eq. (3.6):

$$D_{k+1} = D_k \pm \Delta D \quad (3.6)$$

where D_k and D_{k+1} are the previous and next perturbation of duty cycle respectively, and ΔD is the constant width of the step size. Basically, if the tendency of change in PV voltage and PV

power increase regarding to an increase in the duty cycle, the control system moves in the same direction; otherwise the operating point moves in the opposite direction. The process is continued until it reaches to the MPP and then it oscillates around the optimal MPP. The probabilities of the direction P&O-MPPT algorithm are explained in fig 3.7. In general, there are three main issues facing its operation: a long convergence time, high oscillation around the MPP and a drift problem associated with irradiance changing rapidly. These issues detailed as follows. Clearly, a large ΔD leads to a faster steady state and large oscillations after reaching the MPP[46].

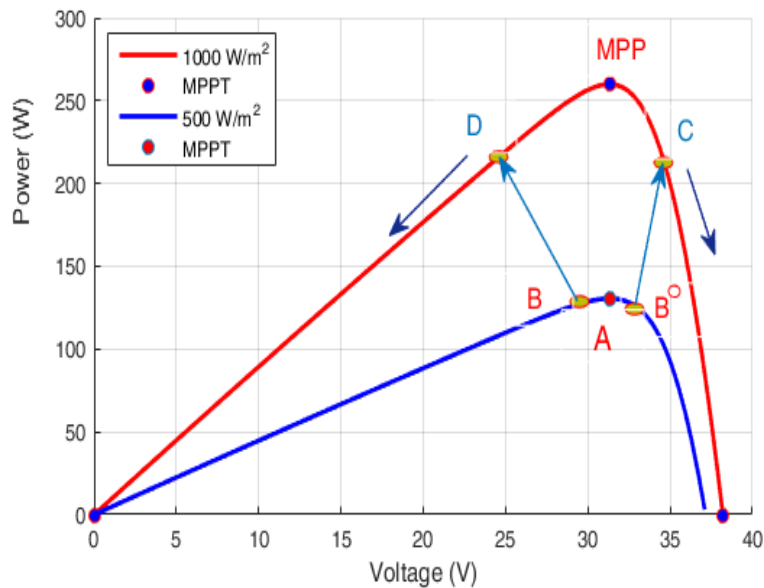


Fig. 3.7: P-V curve for fast irradiation change from A [low point] to D or C [high point] to problem P&O- MPPT.

Conversely, a small ΔD results in a slower steady state and smooth fluctuations. Owing to this, the size of ΔD is considered a crucial issue that needs controlling in the system. Another drawback is loss of the right direction of the algorithm when the weather conditions change rapidly. This phenomenon can happen, as shown in Fig. 3.7. when point A (low point), which represents the MPP at a low irradiance level, is oscillating between B and B⁰ and then moves to point C or D (high point) due to rapid increase in the irradiance. As a result, the right direction of algorithm moves far away from the new MPP, regarding to the principle properties direction of the conventional P&O-MPPT algorithm[54].

3.6 Control Technique

As explained in the previous section, the MPPT algorithm tells a MPPT controller how to move the operating voltage. Then, it is a MPPT controller's task to bring the voltage to a desired level and maintain it. There are several methods often used for MPPT as shown fig 3.7. fuzzy logic and PI control based on P&O method MATLAB Simulink

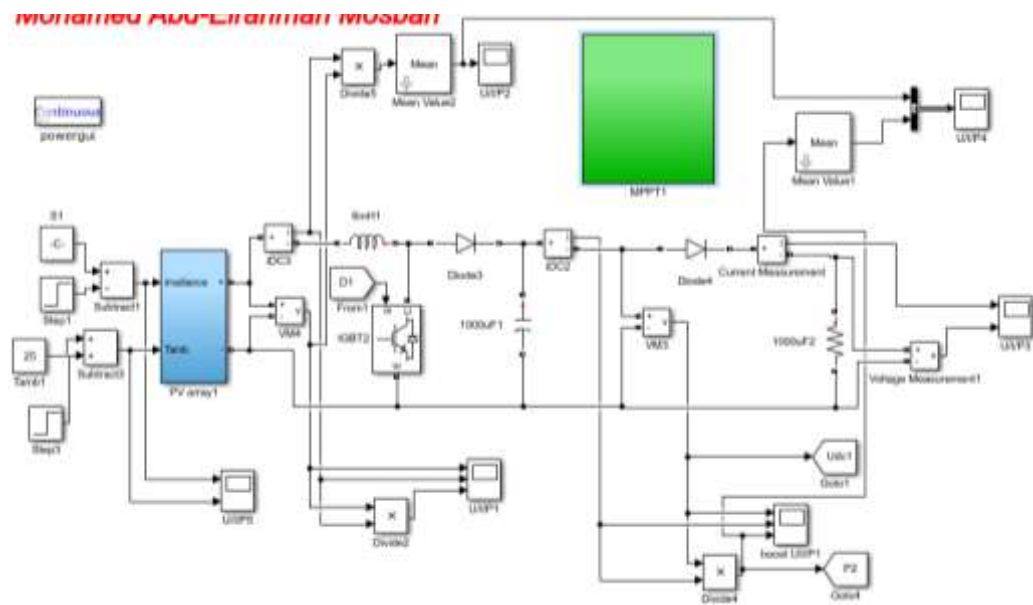


Fig. 3.7: MPPT using fuzzy logic and PI control based on P&O method MATLAB Simulink.

3.6.1 P&O Based on PI

In this method the controller adjusts the voltage by a small amount from the array and measures power, if the power increases, further adjustments in the direction are tried until power no longer increases, this is in addition to exploring the performance of the classical method under fast-changing or ramp changing of solar irradiation or ambient temperature with small or large steps irrespective of the location of the initial operating point to the right or left of the MPP. This is called P&O method[54]. it is the most commonly used MPPT method Hence, this study proposes a modified P&O MPPT with PI control a checking algorithm is introduced. Even though many authors have proposed modifications to P&O method in its conventional form; less focus have been given for P&O particle initialization, P&O with PI controller in MATLAB Simulink the output power solar PV Improvements can be obtained through a digital controller, transforming the conventional P&O into an adaptive solution once different step sizes according to the change distance of the MPP are performed. fig.9 shows a control of boost converter to equal an actual level using a closed-loop control performing the P&O based on PI controller[45]. But less in efficiency than fuzzy logic control based on P&O.

3.6.2 P&O Based on Fuzzy Logic

Nowadays, FL control based on an MPPT technique has become a popular method for PV systems [55]. The structure of FL control includes three stages: fuzzification, fuzzy rules and defuzzification, the fuzzy logic consist of input variables are converted into linguistic variables based on many defined membership functions. In next stage, these linguistics variables get manipulated, according to rules based on the “ifethen” concept that are guided by the desired behavior of the system. In the last stage, the FL control converts the linguistic variables into

numerical variables using the output of membership functions. In general, the quantity of membership functions is considered an important aspect of the design as it determines the speed and accuracy of the FL system [56].

If the system has more membership functions. The implementation problem becomes over complex, resulting in an accurate system but with an excessive processing time. In contrast, if the system has few membership functions, then it is simple and whilst there is a faster processing system time and there is a high acceptable diversity of outcomes.

Table 3.2: fuzzy rules that are used FL-MPPT

Δe	E			
	NS	ZZ	PS	PB
NS	NS	ZZ	PS	ZZ
ZZ	ZZ	PS	PB	PS
PS	PS	PS	PS	PB
PB	PS	PB	PB	PS

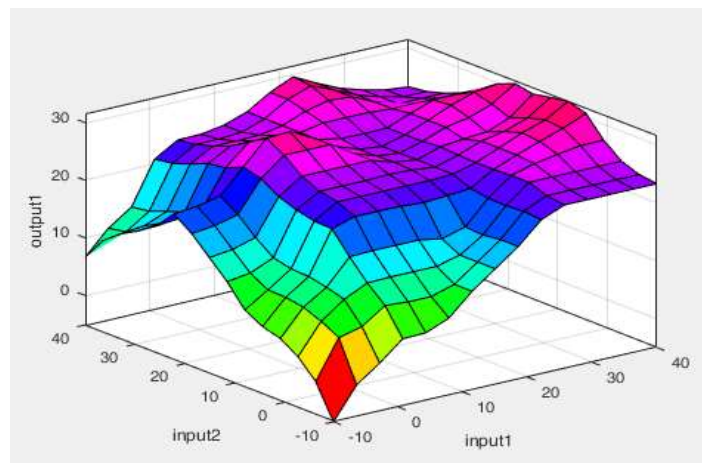


Fig. 3.8: surface of FLC absolute output 3D as a function of the two inputs

The work of the FL-MPPT is to examine the first input, if this value is greater than zero the incremental change of the duty cycle increases until the MPP is reached, whereas if it is less than zero then the opposite occurs until the optimal value is reached. The second input is then used to reduce the oscillation in the duty cycle effectively. The quantity of membership functions of the FL-MPPT method is divided into five values: negative small (NS), Z, Zero (ZZ), positive small (PS), and positive big (PB). For example, if the value of the error is NS and changing error also negative big PB, the predefined rules assign the next variable duty cycle as ZZ, with process

continuing until the optimal MPP is reached. All the rules of the FL-MPPT algorithm are provided in Table 3.2. In general, FL- MPPT is considered one of the most efficient controllers for a PV system due to its smooth fluctuation, and high accuracy in reaching the MPP. In addition, as mentioned earlier, it does not require training data and thus works on different types[55].

3.7 Comparison Between Pi and Fuzzy Logic Based on P&O

Conventional P&O is modified by the introduction of PI controller to improve its performance and fuzzy logic to better controller is then compared with the proposed controller. The comparison is done under both varying temperature and irradiance conditions, mentioned in previous two subsections. The proposed controller clearly outperforms the modified P&O algorithm. The comparison of the generated power.

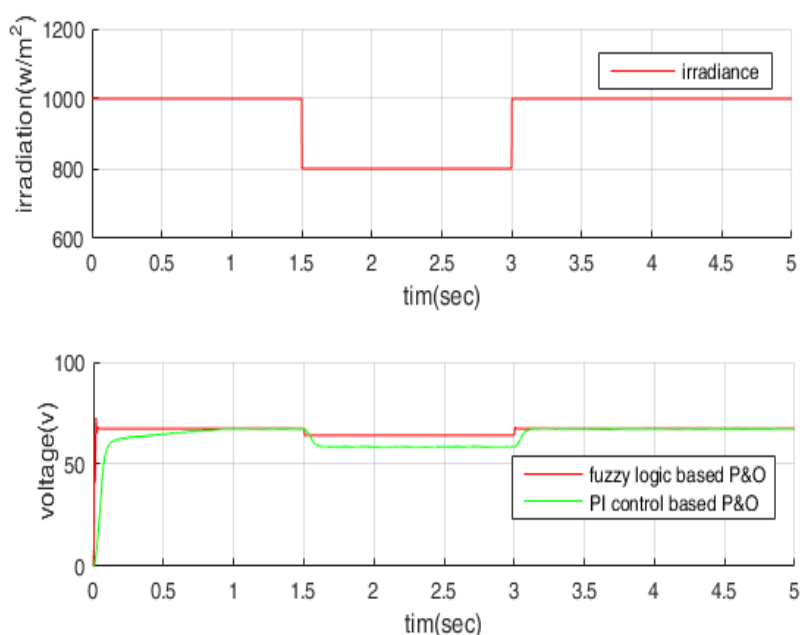


Fig. 3.9: irradiation and comparison between output voltage used fuzzy logic and PI under varying fast change irradiation.

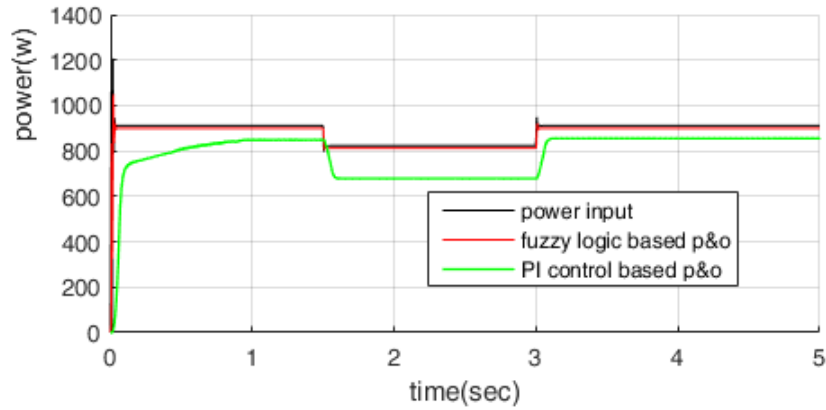


Fig 3.10: comparison between output power used fuzzy logic and PI under varying fast change irradiation

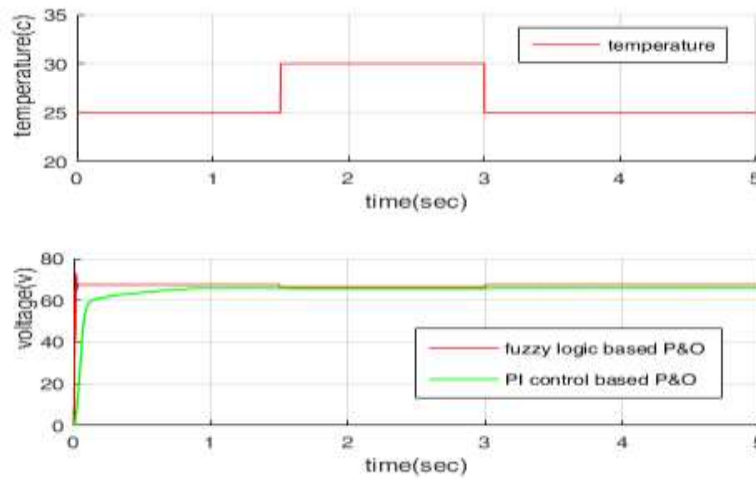


Fig 3.11: temperature and comparison between output voltage used fuzzy logic and PI under varying fast change temperature.

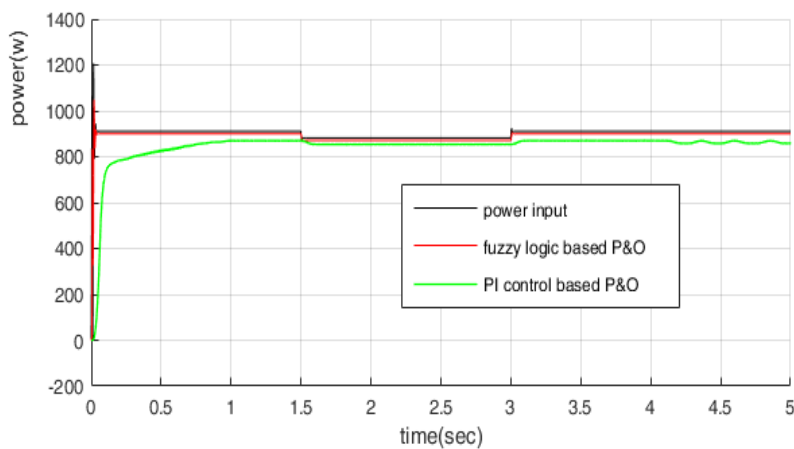


Fig 3.12: comparison between output power used fuzzy logic and PI under varying fast change temperature

under varying temperature is display in Fig. 3.11. Similarly, the power generation comparison under varying irradiance is display in Fig. 3.9. It can be observed that the modified used FL-P&O has improved its performance when compared with the PI-P&O as is much more robust. But it still takes considerable amount of time to reach MPP whenever the array is subjected to massive parameter variations. Moreover, these comparisons also validate the performance of the proposed controller as it is not only tracking the PV array voltage but also achieving MPPT robustly.

3.8 Conclusion

A novel maximum power point tracking technique based on FL-MPPT PV system has been presented, which has the ability to track the MPP when there are big fluctuations of irradiation. The advantages and disadvantages of the FL-MPPT and P&O-MPPT have been discussed. The designed membership functions of FL the controller where tuned based on modified a P&O algorithm to incorporate the advantages of the PI-MPPT and the FL-MPPT as well as to eliminate their drawbacks. A MATLAB-SIMULINK model for the PV system was developed. The P&O-MPPT, FL-MPPT, PI-MPPT and proposed method were simulated, being then compared, according to their common features. The simulation results have revealed that the proposed technique exhibits higher output power, medium oscillation around the MPP point under the steady state condition and no divergence from the MPP during varying (irradiation and temperature, etc.) conditions regardless of the speed of change. That is, the proposed concept has been demonstrated to be highly effective for working with a PV system, achieving efficiencies of around 99.6%. Finally, this modification has been shown to be simple to implement. The fuzzy rules of the proposed method are obtained from a modified P&O- MPPT algorithm. The proposed technique accurately tracks the maximum power point and avoids the driftage problem.

Comparison and Performance Analysis of Unipolar and Bipolar Digitally-Controlled Single-Phase Inverters

4.1 Introduction

Inverters are used in single phase motor drives and uninterruptible AC power supplies. These inverters provide a sinusoidal AC output whose magnitude and frequency can be controlled. There are several doable inverter topologies and switching schemes. Each one of these topologies has its own relative merits and demerits. Efficiency and output current distortion are two main parameters factors governing the selection of inverter system. It is argued that current controlled inverters offer important merits by minimization of current distortion[57]. For using SPWM employing unipolar and bipolar switching with the same frequency, it is found that the bipolar SPWM modulated system is more stable and performs better than the unipolar double-frequency SPWM modulated system. However, the same bipolar and unipolar switching frequency and the stability are maintained for the two systems. The two topologies are used to reduce the output current distortion and the inverter performance (both bipolar SPWM and unipolar SPWM) with filter circuit is presented in[58]. The use of unipolar PWM four leg inverter applied to unsymmetrical two-phase fed induction motor, is investigated for THD in the unbalanced output voltage of the inverter. The planned combination of unipolar and bipolar PWM can improve the current distortion and reduce THD, while still can sustain high efficiency even with the power factors other than unity. The use of space vector pulse width modulation (SVPWM) technique shows a performance better that SPWM technique in respect of power quality [59]. Multi-level inverters are used to reduce the THD in the output voltage waveform without reduction in power output of the inverter with increase in output voltage level. Compared to bipolar switching, unipolar switching has the advantage of lower switching losses and filter size. The concept of sinusoidal pulse width modulation for inverters is explain with analyses extended to different kinds of SPWM strategies in reference [60][61]

Several topologies are used to generate sinusoidal output waveform and reduce THD. The effect of modulation index on THD for sinusoidal waveform is investigated. A triangular carrier comparison based Synchronized SPWM for medium voltage inverters with low switching frequency (less than 500Hz) is proposed in this research. This is proposed in order to have a good dynamic behavior of the synchronization scheme and to reduce THD of the triangular carrier high frequency waveform as well. Also, the output voltage waveform becomes sinusoidal [62].

4.2 Circuit Description and Operation

There are many doable inverter topologies and switching schemes, and each one will have its own relative benefits and downsides. Efficiency and output current distortion are two necessary factors governing the selection of inverter system. two inverter switching strategies are explored. These are the unipolar and bipolar current controlled inverter employing both the SPWM (Sinusoidal Pulse Width Modulation) and the THPWM (Third Harmonic Pulse Width Modulation) techniques. The models of these techniques are simulated using MATLAB-Simulink software. Simulation results are compared with results of an experimental prototype to confirm validity of results[63]. Circuit topology is shown in Fig 4.1. It consists of a direct current (DC) voltage source, four switches, LC output filter and a load connecting to the middle of each arm at the junctions A and B.

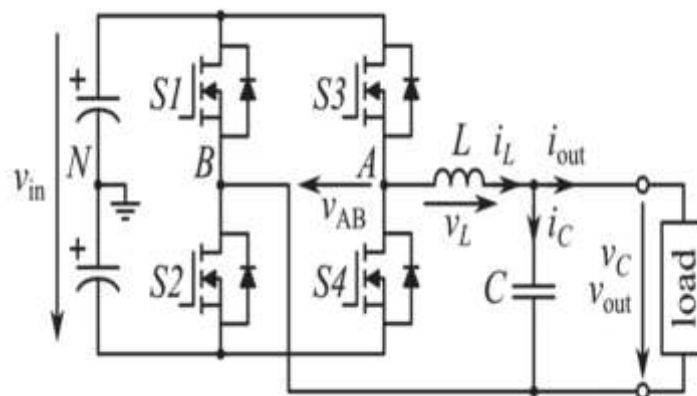


Fig 4.1: Inverter circuit with LC filter

By switching $V(AB)$ between the DC input voltage $+v_{in}$ and $-v_{in}$ with switches (S2, S3) on, (S4, S1) off and (S4, S1) on, (S2, S3) off, a bipolar pulse-width modulation (PWM) is performed. For unipolar pulse-width modulation, it consists of the two more freewheeling switch combinations, $\{S1; S2; S3; S4\} = \{ON; OFF; ON; OFF\}$, $\{S1; S2; S3; S4\} = \{OFF; ON; OFF; ON\}$

that yields $V(AB) = 0$, are used in alternation with active switch combinations. The switching pulses are generated for the used four techniques as follows[62], [64].

4.3 Full- Bridge Single Phase Inverter

A full bridge inverter is shown in fig 4.1. This inverter consists of two one-leg analyzes the performance of unipolar and bipolar current controlled inverter employing both the SPWM (Sinusoidal Pulse Width Modulation) and the THPWM (Third Harmonic Pulse Width Modulation) techniques. The models of these techniques will be simulated using MATLAB-Simulink software and the simulation results will be compared with results of an experimental prototype to confirm validity of the results. The results will be taken for both static and dynamic loads with different modulation index. Inverter is substantially an interface between DC source like photovoltaic cell and AC networks[63][65].

4.3.1 Unipolar Switching Employing SPWM

In this scheme, the switching pulses are generated by comparing two sine-waveforms[66]. have the same magnitude and frequency with phase shift 180° between them - with a triangular carrier waveform as shown in Fig. 4.2.

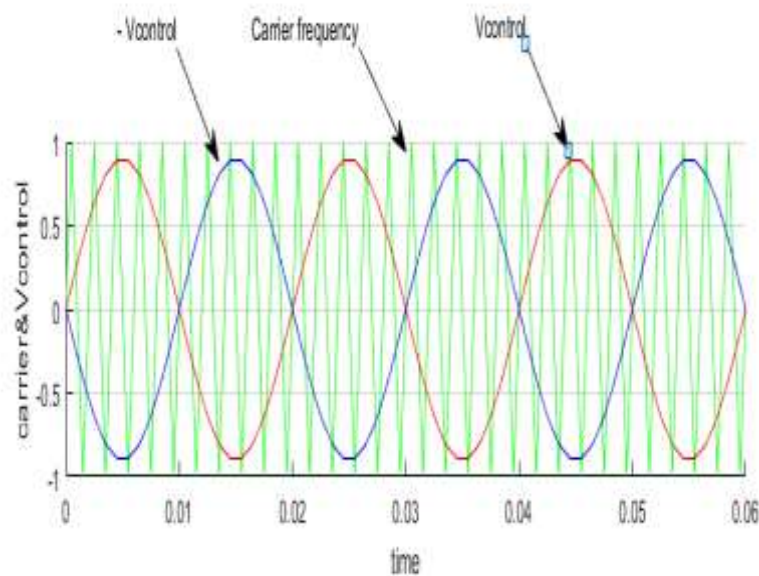


Fig. 4.2: Unipolar switching with SPWM

4.3.2 Unipolar Switching Employing THPWM

In this scheme, the switching pulses are generated by comparing the third harmonic waveform, equals to $\sin \theta + \frac{1}{6} \sin 3\theta$, with a triangular carrier waveform as shown in Fig. 4.3.

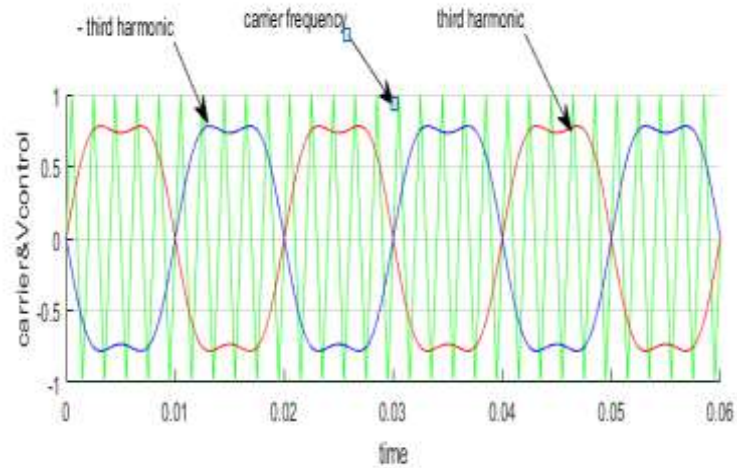


Fig. 4.3: Unipolar switching with THPWM

4.3.3 Bipolar Switching Employing SPWM

In this scheme, the switching pulses are generated by comparing a sine-waveform with a triangular carrier waveform as shown in Fig. 4.4[61].

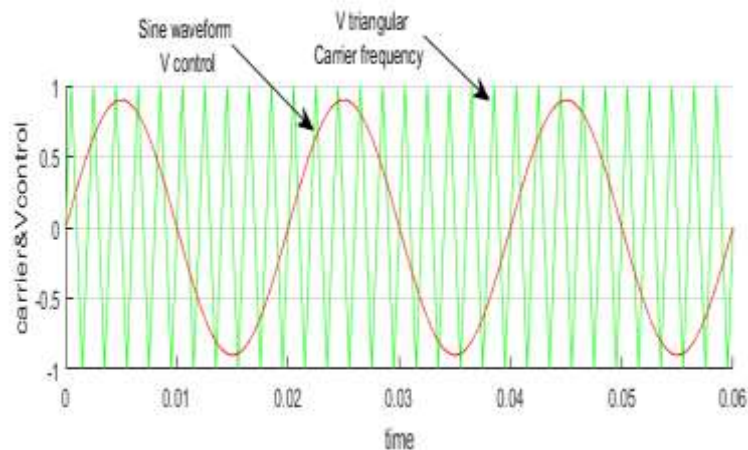


Fig. 4.4: Bipolar switching with SPWM

4.3.4 Bipolar Switching Employing SPWM

In this scheme, the switching pulses are generated by comparing the third harmonic waveform, equals to $\sin \theta + \frac{1}{6} \sin 3\theta$, with a triangular carrier waveform as shown in Fig. 4.5.

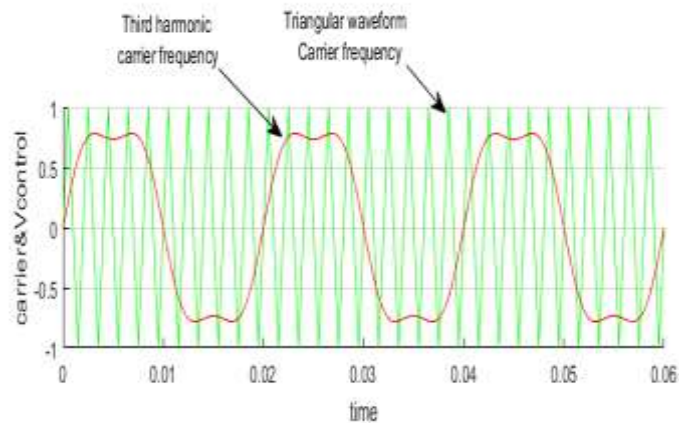


Fig. 4.5: Bipolar switching with THPWM

The performance and switching patterns of the used inverter circuit as shown in Fig. 4.1 have been verified through simulations. A prototype has been implemented to verify the simulation results using the same simulation parameters. The results will be presented and discussed for both static and dynamic loads as follows.

4.4 Static Resistive Load With LC Filter

The specifications of the inverter circuit used for simulations and prototype in Fig. 4.6 are given in Table 4.1.



Fig. 4.6: A picture for the experimental prototype

Table 4.1: Specifications with static load

Parameter	Value
V_{in}	50 V
f_{sw}	500 Hz
f_l	50 Hz
L	5 mH
C	100 μ F
R	22 Ω

4.4.1 SPWM with Unipolar voltage fed Static Resistive Load

The switching patterns as shown in Fig. 4.7. and the output voltage is shown in Fig. 4.8. with LC filter from simulation and in Fig. 4.9. from experimental setup and program in appendix A1. Figure 4.10. as shows the FFT for the inverter output with modulation index of 0.9 with carrier triangular waveform 600 HZ.

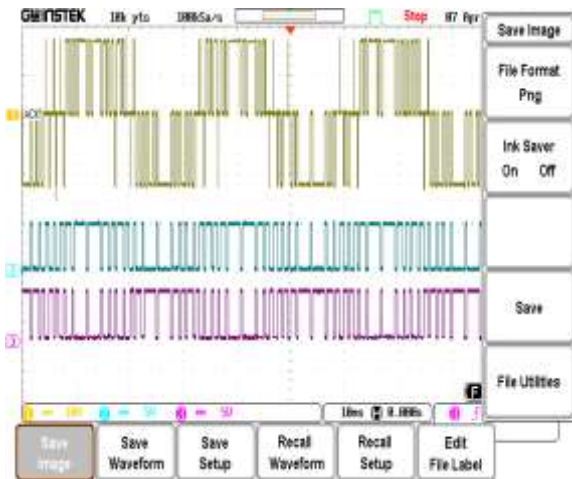


Fig. 4.7: Experimental switching pulses for unipolar switching

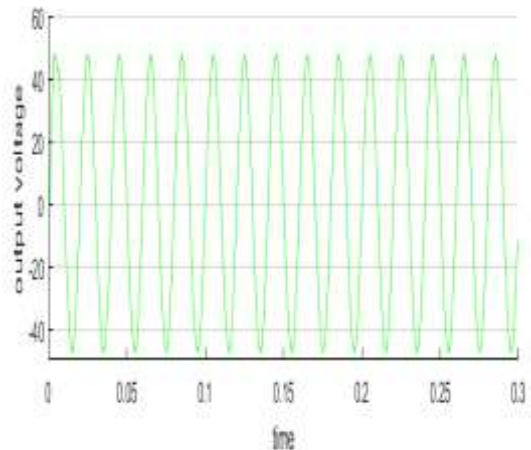


Fig. 4.8: Simulated output voltage with SPWM with LC filter

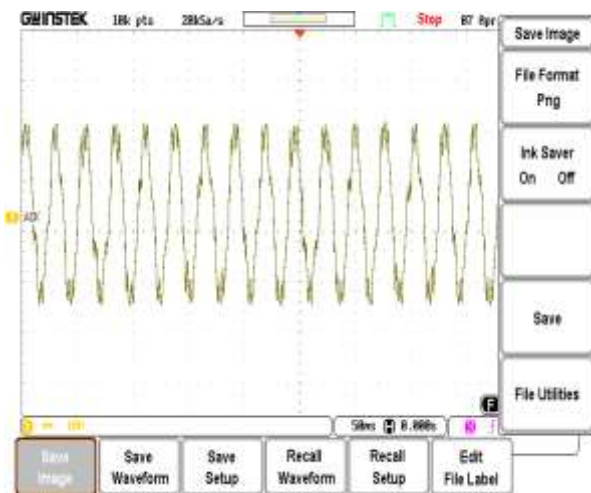


Fig. 4.9: Experimental output voltage with SPWM with LC filter

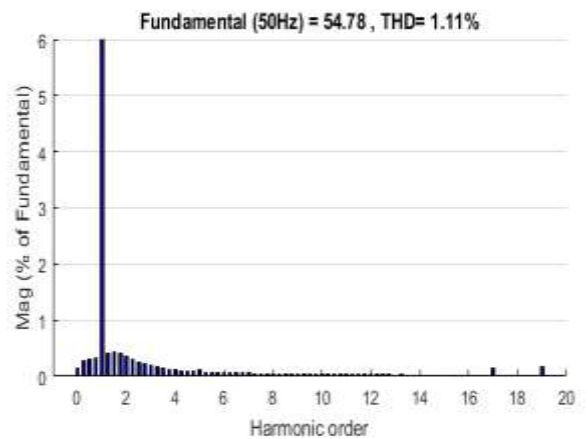


Fig. 4.10: FFT for unipolar switching with SPWM

4.4.2 THPWM with Unipolar voltage fed Static Resistive Load

The switching patterns are shown in Fig. 4.11 and the output voltage as shown in Fig. 4.12 from simulation with LC filter and in Fig. 4.13 from experimental setup and program in appendix A2. Figure 4.14 shows the FFT for the inverter output with modulation index of 0.9 with carrier triangular waveform 600 HZ.

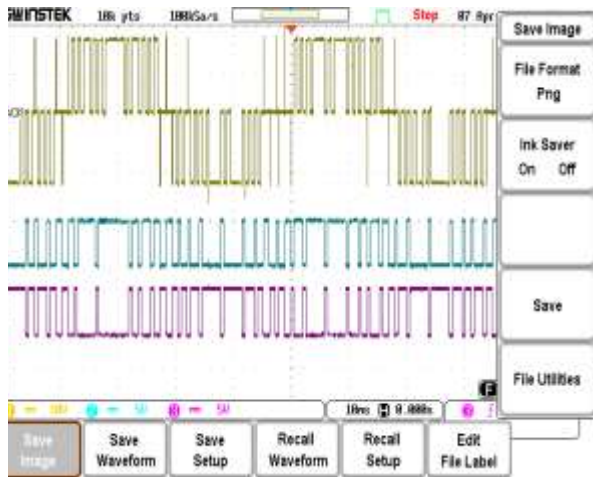


Fig. 4.11: Experimental switching pulses for unipolar switching with THPWM

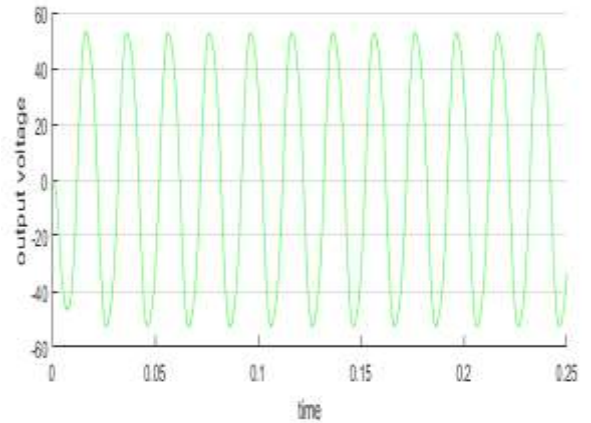


Fig. 4.12: Simulated output voltage with LC filter

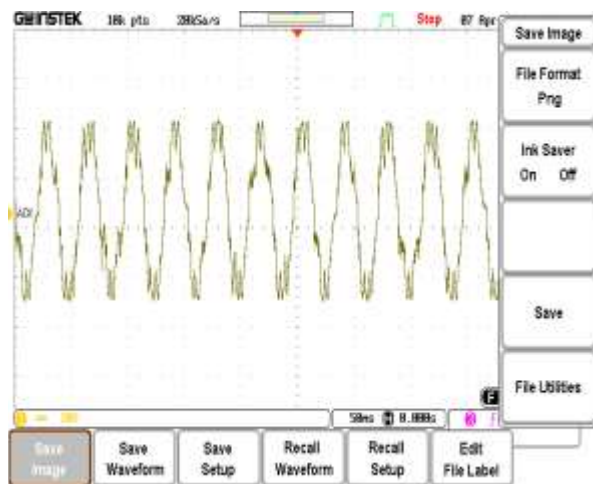


Fig. 4.13: Experimental output voltage

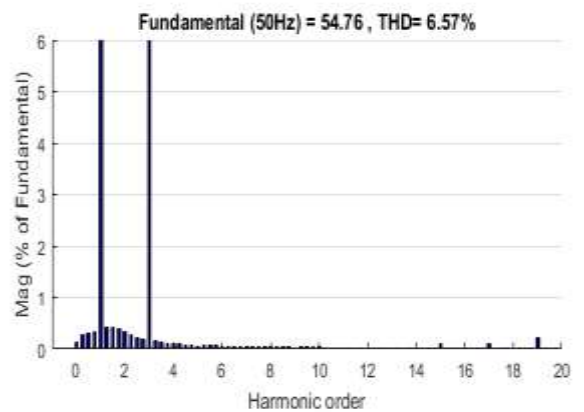


Fig. 4.14: FFT for unipolar switching with THPWM

4.4.3 SPWM with Bipolar voltage fed Static Resistive Load

The switching patterns SPWM with Bipolar as shown in Fig. 4.15. and the output voltage as shown in Fig. 4.16 from simulation with LC filter and in Fig. 4.17. from experimental setup and program in appendix A3. Figure 4.18. shows the FFT for the inverter output with modulation index of 0.9 with carrier triangular waveform 600 HZ.

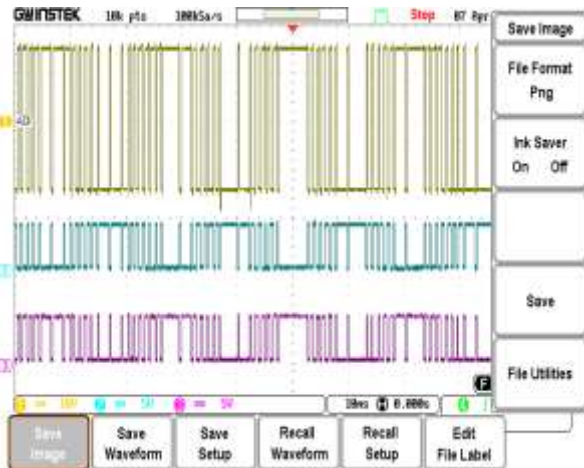


Fig. 4.15: Experimental switching pulses for bipolar switching with SPWM

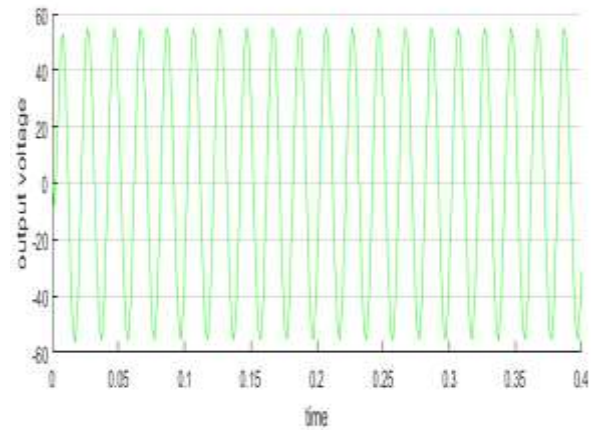


Fig. 4.16: Simulated output voltage

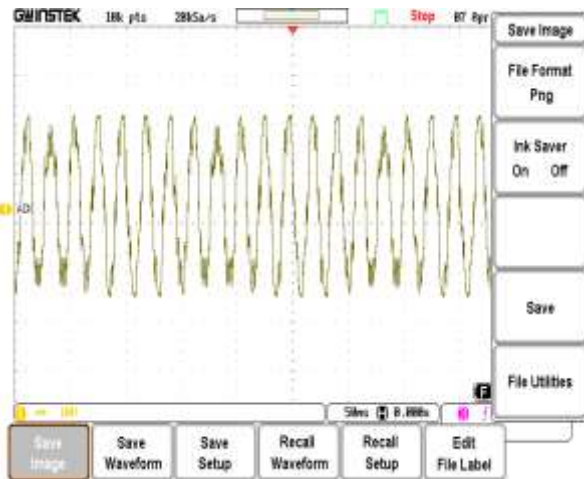


Fig. 4.17: Experimental output voltage

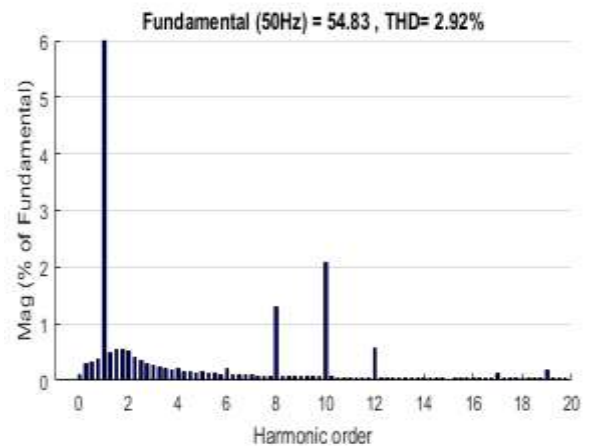


Fig. 4.18: FFT for bipolar switching with SPWM

4.4.4 THPWM with Bipolar voltage fed Static Resistive Load

The switching THPWM with Bipolar patterns as shown in Fig. 4.19. and the output voltage is shown in Fig. 4.20. from simulation and in Fig. 4.21. from experimental setup and program in appendix A4. Figure 4.22. shows the FFT for the inverter output with modulation index of 0.9 with carrier triangular waveform 600 HZ.

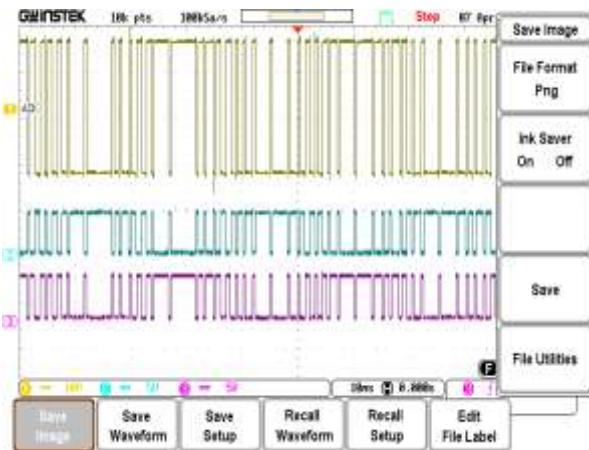


Fig. 4.19: Experimental switching pulses for bipolar switching with THPWM

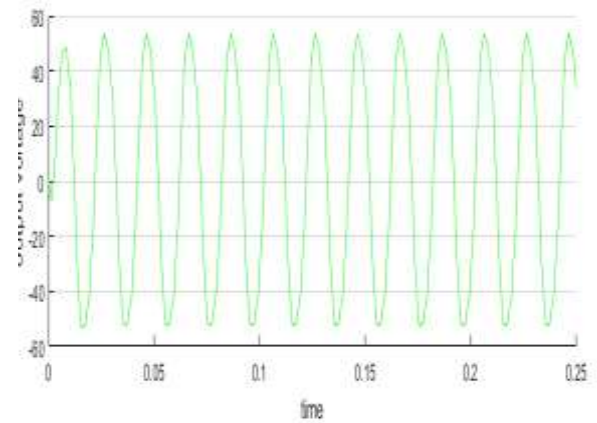


Fig. 4.20: Simulated output voltage with LC filter

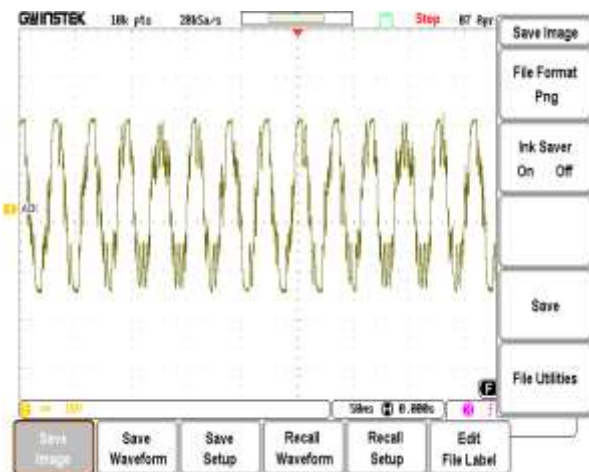


Fig. 4.21: Experimental output voltage with LC filter

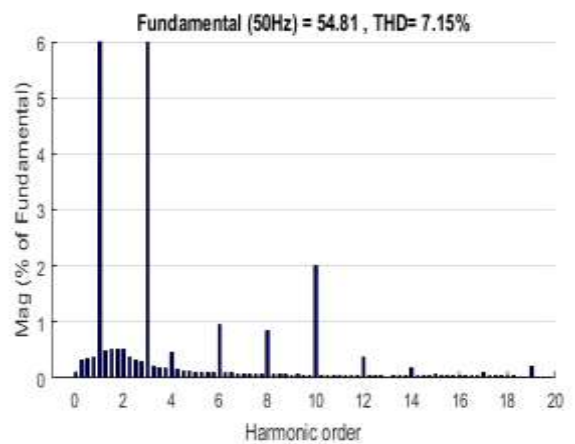


Fig. 4.22: FFT for bipolar switching with THPWM

4.5 Dynamic load with LC filter

The specifications of the inverter circuit used for simulations and prototype in Fig. 4.23. are given in Table 4.2. For inverter output with modulation index of 0.9 with carrier triangular waveform 600 HZ.



Fig. 4.23: A picture for the experimental prototype single phase inverter

Table 4.2: Specifications with dynamic load

Parameter	Value
V_{in}	100 V
f_{sw}	500 Hz
f_l	50 Hz
L	5 mH
C	100 μ F
L_{main}	62 mH
$L_{auxiliary}$	0.9 μ H
C_{run}	20 μ F

4.5.1 Unipolar switching Dynamic load with SPWM

The output current Unipolar switching Dynamic load with SPWM as shown in Fig. 4.24. from simulation and in Fig. 4.26. from experimental setup. Figure 4.25. shows the FFT for the inverter output with modulation index of 0.9 with carrier triangular waveform 600 HZ.

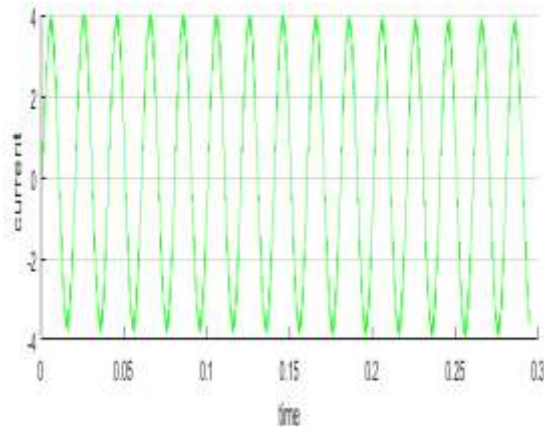


Fig. 4.24: Simulated output current with LC filter for unipolar switching with SPWM

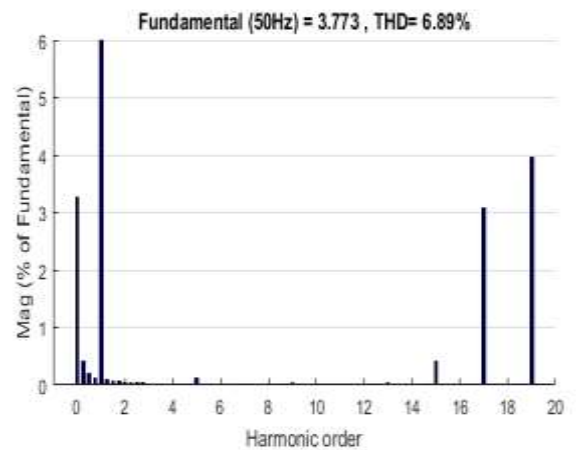


Fig. 4.25: FFT for unipolar switching with SPWM

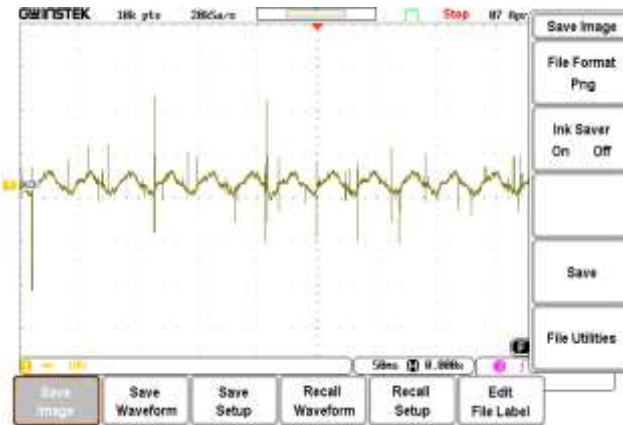


Fig. 4.26: Experimental output current with LC filter for unipolar switching with SPWM

4.5.2 Unipolar switching Dynamic load with THPWM

The output current is shown Unipolar switching Dynamic load with THPWM as shown in Fig. 4.27. from simulation and in Fig. 4.29. from experimental setup. Figure 4.28. shows the FFT for the inverter output with modulation index of 0.9 with carrier triangular waveform 600 HZ.

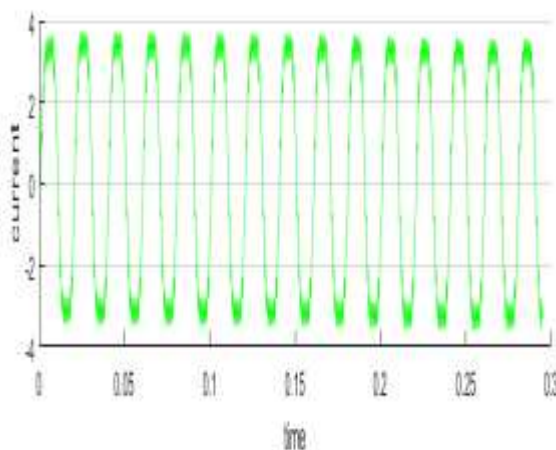


Fig. 4.27: Simulated output current with LC filter for unipolar switching with THPWM

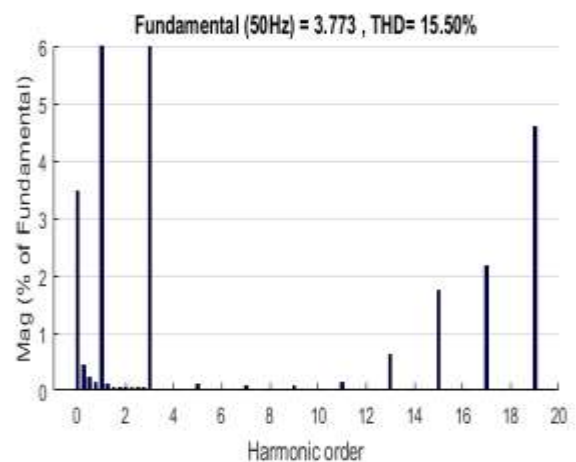


Fig. 4.28: FFT for unipolar switching with THPWM

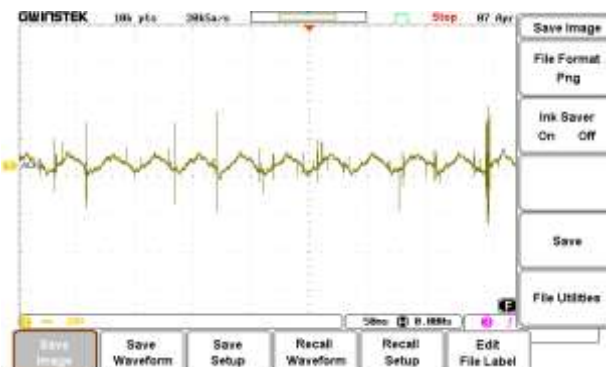


Fig. 4.29: Experimental output current with LC filter for unipolar switching with THPWM

4.5.3 Bipolar switching Dynamic load with SPWM

The output current is shown Bipolar switching Dynamic load with SPWM as shown in Fig. 4.30. from simulation and in Fig. 4.32. from experimental setup. Figure 4.31. shows the FFT for the inverter output with modulation index of 0.9 with carrier triangular waveform 600 HZ.

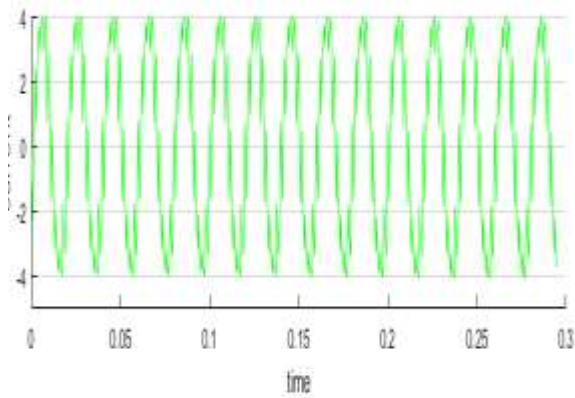


Fig. 4.30: Simulated output current with LC filter for Bipolar switching with SPWM

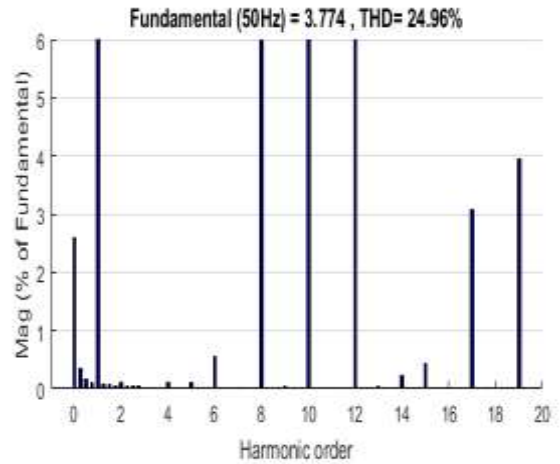


Fig. 4.31: FFT for Bipolar switching with SPWM

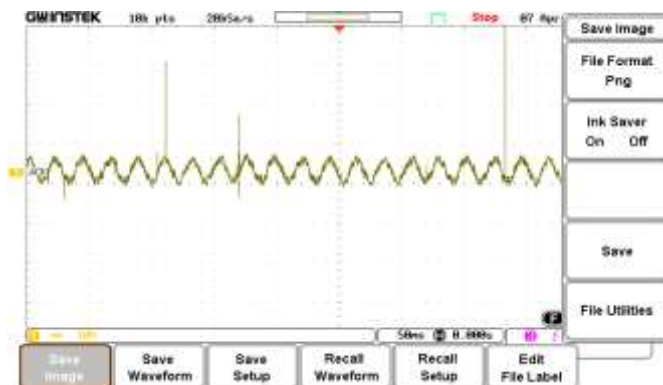


Fig. 4.32: Experimental output current with LC filter for Bipolar switching with SPWM

4.5.4 Bipolar switching Dynamic load with THPWM

The output current is shown Bipolar switching Dynamic load with THPWM as shown in Fig. 4.33. from simulation and in Fig. 4.35. from experimental setup. Figure 4.34. shows the FFT for the inverter output with modulation index of 0.9 with carrier triangular waveform 600 HZ.

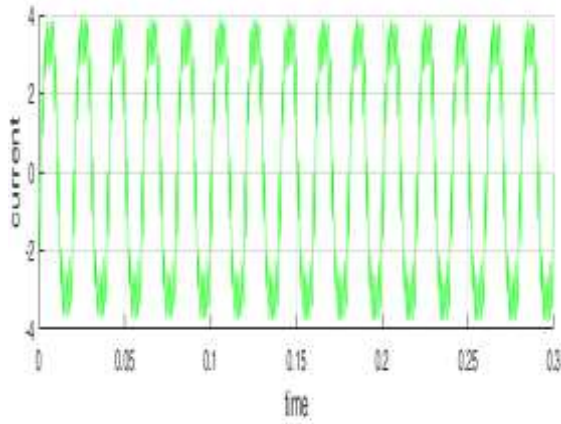


Fig. 4.33: Simulated output current with LC filter for Bipolar switching with THPWM

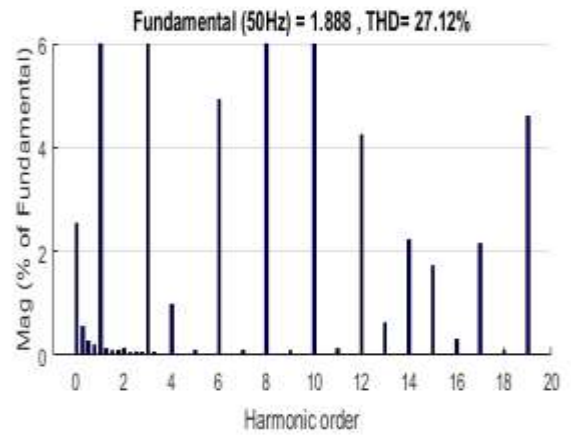


Fig. 4.34: FFT for Bipolar switching with THPWM

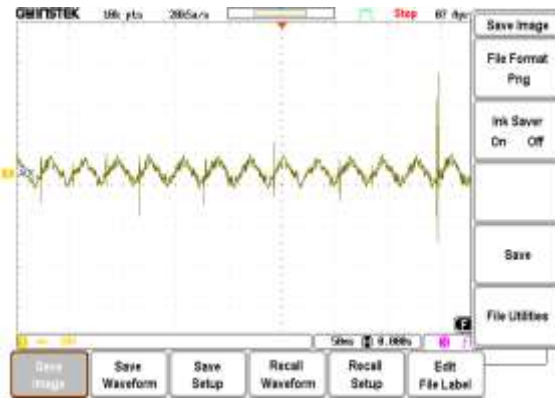


Fig. 4.35: Experimental output current with LC filter for Bipolar switching with THPWM

4.6 Comparison Between the Four Techniques

These are the unipolar and bipolar current controlled inverter employing both the SPWM (Sinusoidal Pulse Width Modulation) and the THPWM (Third Harmonic Pulse Width Modulation) techniques. The models of these techniques are simulated using MATLAB-Simulink software. Simulation results are compared with results of an experimental prototype to confirm validity of results. The results are taken for both static and dynamic loads with different modulation index. Both simulated and experimental results are in a good agreement. The results showed that the unipolar switched inverter offers low current distortion over bipolar switched inverter[67], [68].

4.6.1 Inverter Fed Static Resistive Load With LC Filter

Figure 4.36. shows the variation of THD with the four investigated techniques for different modulation ratios in case of static resistive load with LC filter. It is observed that SPWM technique with unipolar switching gives the least THD. Also, SPWM technique with bipolar switching gives THD less than THPWM technique with unipolar switching.

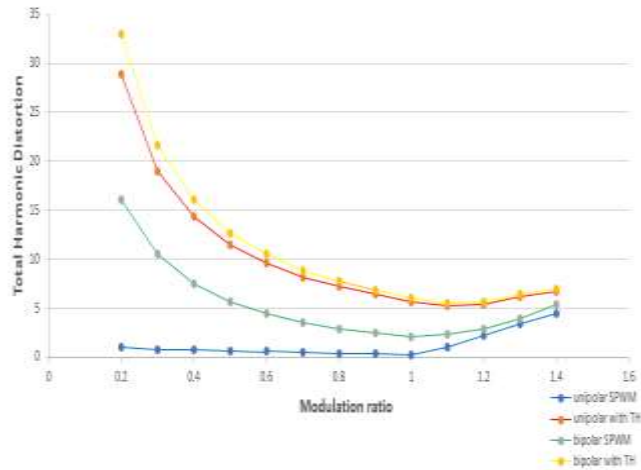


Fig. 4.36: THD for static resistive load with LC filter

4.6.2 Inverter Fed Dynamic Load With LC Filter

Figure 4.37. shows the variation of THD with the four investigated techniques for different modulation ratios in case of dynamic single-phase induction motor load with LC filter. It is observed that SPWM technique with unipolar switching gives the least THD. Also, THPWM technique with unipolar switching gives THD less than SPWM technique with bipolar switching.

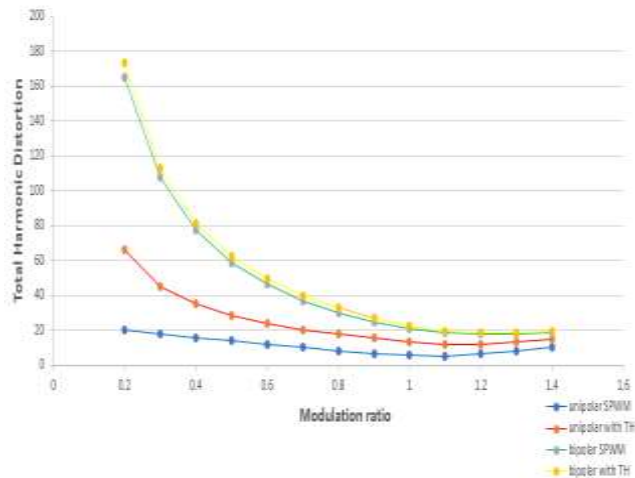


Fig. 4.37: THD for dynamic load with LC filter

4.7 conclusion

In this paper, a comparison between unipolar and bipolar PWM techniques is introduced employing SPWM and THPWM with various modulation ratio. The comparison between the presented four topologies is presented for static and dynamic loads. The models of these topologies are implemented by simulations and an experimental prototype. For static load, SPWM technique with unipolar switching gives the least THD whereas SPWM technique with bipolar switching gives THD less than THPWM technique with unipolar switching. For dynamic load, also SPWM technique with unipolar switching gives the least THD whereas THPWM technique with unipolar

switching gives THD less than SPWM technique with bipolar switching. The simulated and experimental results were in a good agreement.